

The Unusual Temporal and Spectral Evolution of the Type IIIn Supernova 2011ht¹

P. W. A. Roming^{2,3}, T. A. Pritchard³, J. L. Prieto^{4,5}, C. S. Kochanek^{6,7}, C. L. Fryer^{8,9,10},
K. Davidson¹¹, R. M. Humphreys¹¹, A. J. Bayless², J. F. Beacom^{6,7,12}, P. J. Brown¹³, S. T.
Holland¹⁴, S. Immler^{15,16,17}, N. P. M. Kuin¹⁸, S. R. Oates¹⁸, R. W. Pogge^{6,7}, G.
Pojmanski¹⁹, R. Stoll⁶, B. J. Shappee^{6,20}, K. Z. Stanek^{6,7}, D. M. Szczygiel⁶

ABSTRACT

We present very early UV to optical photometric and spectroscopic observations of the peculiar Type II_n supernova (SN) 2011ht in UGC 5460. The UV observations of the rise to peak are only the second ever recorded for a Type II_n SN and are by far the most complete. The SN, first classified as a SN impostor,

¹This paper is dedicated to our colleague, Weidong Li, who died on 2011-12-12. His contribution to the study of all types of SNe was tremendous.

²Space Science & Engineering Division, Southwest Research Institute, P.O. Drawer 28510, San Antonio, TX 78228-0510, USA; Corresponding author's e-mail: proming@swri.edu

³Department of Astronomy & Astrophysics, Penn State University, 525 Davey Lab, University Park, PA 16802, USA

⁴Department of Astrophysical Sciences, Princeton University, Peyton Hall, Princeton, NJ 08544, USA

⁵Hubble and Carnegie-Princeton Fellow

⁶Department of Astronomy, The Ohio State University, 140 W. 18th Ave., Columbus, OH 43210, USA

⁷Center for Cosmology & AstroParticle Physics, The Ohio State University, 191 W. Woodruff Ave., Columbus, OH 43210, USA

⁸CCS-2, MS D409, Los Alamos National Laboratory, Los Alamos, NM, 87544, USA

⁹Physics Department, University of Arizona, Tucson, AZ 85721, USA

¹⁰Physics and Astronomy Department, University of New Mexico, Albuquerque, NM 87131, USA

¹¹Minnesota Institute for Astrophysics, University of Minnesota, 116 Church St. S.E., Minneapolis, MN 55455, USA

¹²Department of Physics, The Ohio State University, 191 W. Woodruff Ave., Columbus, OH 43210, USA

¹³Department of Physics & Astronomy, University of Utah, 201 James Fletcher Bldg., 115 S. 1400 E. 201, Salt Lake City, UT 84112-0830, USA

¹⁴Space Telescope Science Center, 3700 San Martin Dr., Baltimore, MD 21218, USA

¹⁵Astrophysics Science Division, NASA Goddard Space Flight Center, Greenbelt, MD 20771, USA

¹⁶Center for Research & Exploration in Space Science & Technology, NASA Goddard Space Flight Center, Greenbelt, MD 20771, USA

¹⁷Department of Astronomy, University of Maryland, College Park, MD 20742, USA

¹⁸Mullard Space Science Laboratory, University College London, Holmbury St. Mary, Dorking, Surrey RH5 6NT, UK

¹⁹Warsaw University Astronomical Observatory, Al. Ujazdowskie 4, 00-478 Warsaw, Poland

²⁰National Science Foundation Fellow

slowly rose to a peak of $M_V \sim -17$ in ~ 55 days. In contrast to the ~ 2 magnitude increase in the v -band light curve from the first observation until peak, the UV flux increased by >7 magnitudes. The optical spectra are dominated by strong, Balmer emission with narrow peaks (FWHM ~ 600 km s $^{-1}$), very broad asymmetric wings (FWHM ~ 4200 km s $^{-1}$), and blue shifted absorption (~ 300 km s $^{-1}$) superposed on a strong blue continuum. The UV spectra are dominated by Fe II, Mg II, Si II, and Si III absorption lines broadened by ~ 1500 km s $^{-1}$. Merged X-ray observations reveal a $L_{0.2-10} = (1.0 \pm 0.2) \times 10^{39}$ erg s $^{-1}$. Some properties of SN 2011ht are similar to SN impostors, while others are comparable to Type IIn SNe. Early spectra showed features typical of luminous blue variables at maximum and during giant eruptions. However, the broad emission profiles coupled with the strong UV flux have not been observed in previous SN impostors. The absolute magnitude and energetics ($\sim 2.5 \times 10^{49}$ ergs in the first 112 days) are reminiscent of normal Type IIn SN, but the spectra are of a dense wind. We suggest that the mechanism for creating this unusual profile could be a shock interacting with a shell of material that was ejected a year before the discovery of the SN.

Subject headings: supernovae: individual (SN 2011ht)

1. Introduction

Type IIn supernovae (SNe IIn), a designation first proposed by Schlegel (1990), are characterized by spectra with a narrow H α emission line superimposed on a broad emission component (Chandra et al. 2009) that lacks a broad P-Cygni absorption feature (Pastorello et al. 2002). Most SNe IIn are core collapse events that are due to shock interaction of the ejecta with the circumstellar material (CSM; Chugai 1990; Pastorello et al. 2002; Smith et al. 2008; Chandra et al. 2009), although some thermonuclear explosions are thought to detonate in a hydrogen-rich environment producing SNe IIn-like events (cf. Hamuy et al. 2003; Pastorello et al. 2005; Prieto et al. 2007). As the shock interacts and heats the dense CSM, there is a rapid increase in the production of UV photons.

SNe IIn are a very heterogeneous group (e.g. Chandra et al. 2009; Ofek et al. 2010; Kiewe et al. 2010) ranging from the most luminous SNe (e.g. SN 2006gy with $M_V \simeq -22$ and SN 2008am with $M_R \simeq -22.3$; Smith et al. 2007; Chatzopoulos et al. 2011) to some of the fainter (e.g. SNe 1997bs and 2008S with $M_V \simeq -13$ and $M_R \simeq -13.9$, respectively; Van Dyk et al. 2000; Smith et al. 2009). The nature of the fainter objects, such as SNe 1997bs and 2008S, is unclear (Van Dyk et al. 2000; Smith et al. 2009). Many argue

that they are non-terminal outbursts as opposed to core collapse objects (e.g. Smith et al. 2009) and have been designated “supernova impostors” (Van Dyk et al. 2000). The great eruption of η Car is frequently cited as a Galactic analogue. However, this may be misleading since the great eruption of η Car was an unusual event and none of the extragalactic impostors resemble it in terms of kinetic energy and duration (see Smith et al. 2011b; Kochanek 2011a; Kochanek et al. 2012). Although some impostors are clearly non-terminal events (e.g. η Car, P-Cygni, SN 2000ch), it is not clear that this is the case for all fainter outbursts (cf. Prieto et al. 2008; Botticella et al. 2009; Thompson et al. 2009; Kochanek 2011b, but see Humphreys et al. 2011). For the brighter SNe IIn, there is mounting evidence that the progenitor is a massive, luminous star that retains its hydrogen-shell until shortly before explosion and that the terminal mass loss event is strongly correlated with the death of the star (Gal-Yam et al. 2007; Smith et al. 2011b; Kochanek 2011a).

With the emergence of dedicated supernovae (SNe) follow-up programs and telescopes (e.g. Filippenko et al. 2001; Bloom et al. 2006; Hamuy et al. 2006; Quimby 2006; Drake et al. 2009; Law et al. 2009; Rau et al. 2009), SNe IIn are now being studied more frequently in both the optical and near-IR (e.g. Pastorello et al. 2002; Prieto et al. 2008; Smith et al. 2008, 2009; Drake et al. 2010; Kiewe et al. 2010; Smith et al. 2010a; Drake et al. 2011; Smith et al. 2011a). UV studies, on the other-hand, have seriously lagged behind the redder wavelengths, even though the UV is a promising probe of these interesting objects. Unlike other classes of SNe, SNe IIn are very bright in the UV and can be found in $z > 2$ optical surveys while Type Ia SNe have much redder spectra (Panagia 2003; Cooke et al. 2009). Their intrinsic brightness and long-lived emission also aid in spectroscopically confirming such distant SNe (Cooke 2008). Since they are associated with massive stars and because of their intrinsic UV brightness, SNe IIn are potentially strong probes of star formation and galaxy evolution out to relatively large redshifts ($z > 2$; Cooke 2008).

Previous to 2005, only three SNe IIn had been observed in the UV (SNe 1988Z, 1994Y, and 1998S; Brown 2009), and only a handful since¹. However, none of these SNe were observed early enough to detect the rise in the UV light curve (despite the rapid follow-up after discovery in the case of *Swift* UVOT observed SNe IIn). Recently, the SN IIn PTF09uj was caught on the rise (~ 1.8 mag in ~ 4 days based on two UV detections; Ofek et al. 2010). This rapid UV rise was attributed to the supernova (SN) shock breaking through a dense CSM.

In this paper, we describe SN 2011ht, where the rise in the UV was captured in far greater detail, with over 10 UV observations before peak. Unlike PTF09uj, the rise to peak

¹see http://swift.gsfc.nasa.gov/docs/swift/sne/swift_sn.html

for SN 2011ht was large (~ 7 mag) and slow (~ 40 days). In Section 2, we present the UV to optical photometric and spectroscopic observations, X-ray observations, pre-explosion images, and the host galaxy properties. In Section 3, we review the UV/optical light curves, blackbody fits, and spectral properties. In Section 4, we discuss our results including a comparison to other SN impostors and SNe IIn, as well as model interpretations. In Section 5, we summarize our conclusions.

2. Observations

2.1. Discovery

SN 2011ht (Figure 1) was discovered on 2011-09-29.182 (UT; JD 2455833.682) in the nearby galaxy ($z = 0.0036$) UGC 5460 at (J2000) R.A. = $10^h 08^m 10^s.58$, Dec. = $+51^\circ 50' 57''.5$ with a magnitude of 16.9 (Boles et al. 2011). An ALFOSC spectrum taken with the Nordic Optical Telescope on 2011-09-30.22 suggested that the object was a “SN impostor” with properties similar to the “giant eruption” (see Humphreys & Davidson 1994) of the luminous blue variable UGC 2773-OT (Pastorello et al. 2011). The object was designated PSN J10081059+5150570. On 2011-10-18, Roming et al. (2011) reported UV ($uvw2$, $uvm2$, and $uvw1$), u , b , and v -band brightenings of ~ 4 , ~ 3 , ~ 1.5 and ~ 1.5 magnitudes, respectively. The transient also brightened another 0.4 mag between 2011-10-22 and 2011-10-29, to $V \sim 14.7$. At a distance of 19.2 Mpc for the host galaxy UGC 5460 (Pastorello et al. 2011), this corresponds to an absolute magnitude of $M_V \sim -17$ that is typical of a core-collapse SN (Li et al. 2011). Based in part on this high luminosity, Prieto et al. (2011a) suggested that PSN J10081059+5150570 was a SNe IIn rather than an impostor. Spectroscopic observations on 2011-11-11.5 revealed that the emission profiles were similar to some SNe IIn (Prieto et al. 2011b).

2.2. Photometric Data

Photometric observations were obtained with the *Swift* (Gehrels et al. 2004) Ultra-Violet/Optical Telescope (UVOT; Roming et al. 2005, 2004, 2000) and the All Sky Automated Survey (ASAS-SN) North telescope located on Haleakala, Hawaii. The photometric observations with the UVOT began on 2011-10-4.9, 5.8 days after the initial discovery. The observations were obtained for the three optical filters (ubv) and the three UV filters ($uvw2$, $uvm2$, $uvw1$: $\lambda_c = 1928, 2246, 2600$ Å, respectively; Poole et al. 2008) with a median cadence of three days. Photometry was performed using a $3''$ source aperture following the method

outlined in Brown et al. (2009). A $20''$ aperture centered on a region in the galaxy with a similar background to SN 2011ht was used for galaxy subtraction. The data reduction pipeline used the HEASOFT 6.6.3 (which includes time-dependent sensitivity corrections) and *Swift* Release 3.3 analysis tools with updated UVOT zero-points from Breeveld et al. (2010) to calibrate the resulting photometry (Table 1). The UVOT light curves and the corresponding color evolution are shown in Figure 2. We note that there is a $+0.076$ ($\sigma = 0.052$), $+0.010$ ($\sigma = 0.049$), and 0.068 ($\sigma = 0.027$) magnitude (3σ confidence limit) offset between the UVOT and SDSS u , b , and v filters, respectively (Roming et al. 2009).

We also obtained V -band photometric observations (Figure 2) of SN 2011ht using the commissioning data from the recently installed, 2×14 -cm diameter ASAS-SN telescope. We used ASAS-SN Unit1, equipped with a FLI ProLine CCD camera with Fairchild Imaging $2k \times 2k$ thinned CCD, giving a 4.47×4.47 square-degree field-of-view, corresponding to $7.8''$ /pixel image scale. Because such a large image scale leads to a significant flux contamination by the host galaxy, we estimated the amount of contamination using the *Swift* satellite data and used this to set the baseline of the ASAS-SN photometry.

2.3. Spectroscopic Data

Spectroscopic observations were obtained with the Hobby Eberly Telescope (HET; Ramsey et al. 1998) Low Resolution Spectrograph (LRS; Hill et al. 1998), *Swift* UVOT UV grism (uvgrism), Astrophysical Research Consortium (ARC) telescope Dual Imaging Spectrograph (DIS), and Large Binocular Telescope (LBT) Multi-Object Double Spectrograph #1 (MODS1; Pogge et al. 2010). Dates and exposure times for each of the instruments are provided in Table 2 and the corresponding spectra are shown in Figure 3.

The HET spectra were obtained on 2011-11-01, 2011-11-16, and 2011-12-21. The HET/LRS was used with a $2''$ slit ($R \approx 300$; $\Delta\lambda \approx 4,500 - 10,000 \text{ \AA}$). Standard IRAF² reduction techniques of bias subtraction, flat fielding, and wavelength calibration were used. Relative flux calibration was performed using the flux standards GD191B2B and HD84937 (Fukugita et al. 1996; Massey & Gronwall 1990).

The *Swift* UVOT observations of SN 2011ht included grism observations. On 2011-11-02 and 2011-11-13, four exposures for a total of 3710s and thirteen exposures for a total of

²IRAF is distributed by the National Optical Astronomy Observatory, which is operated by the Association of Universities for Research in Astronomy (AURA) under cooperative agreement with the National Science Foundation.

15,551 s were completed, respectively. The data for the individual exposures were extracted using the new UVOT grism wavelength calibration (Kuin et al., in prep) and the current flux calibration from the *Swift* UVOT CALDB (version 20110731). Based on this calibration, the accuracy of the wavelength scale is typically 15 Å. The individual exposures were summed after rotating the images along the dispersion direction and alignment of the anchor positions. The anchor positions were defined by the 2600 Å line observed in first order. Taking into account the curvature of the spectrum, the spectrum was then extracted from the summed image using a slit width of 1σ of the cross-dispersion Gaussian.

The errors in the flux due to noise are low for wavelengths $\gtrsim 1900$ Å, but the signal-to-noise (S/N) is <3 below 1910 Å and 1770 Å (which is approximately where the sensitivity in the grism begins to drop off) for the 2011-11-02 and 2011-11-13 spectra, respectively. The position of the spectra on the detector was such that a large portion of the second order spectrum lies next to the first order spectrum at wavelengths less than 3600 Å and partially overlaps at 4550 Å. At this point the contaminating flux due to the second order is estimated to be about 12% of the total flux.

We also obtained a spectrum of SN 2011ht on 2011-11-11.5 with DIS on the 3.5m ARC telescope at the Apache Point Observatory (APO). The observations were done with the B400/R300 low-resolution gratings and a 1''5 slit, which give a wavelength coverage from $\sim 3500 - 9600$ Å with a FWHM resolution of 7 Å. Standard IRAF tasks were used to reduce the spectrum. The data were calibrated using a HeNeAr lamp and standard star observations taken on the same night. The strongest telluric lines were corrected using the spectrophotometric standards.

On 2011-11-17.5 spectra were obtained with the MODS1 instrument using a 1''0 wide slit and the G400L and G750L gratings in the Blue and Red channels, respectively. The observations were done in a sequence of three 300 s integrations for a total integration time of 900 s. The slit was oriented along the mean parallactic angle during the exposures ($PA = -140$ deg) since the MODS1 spectrograph does not have an atmospheric dispersion corrector (ADC). The seeing during the exposures was 0''6 FWHM, giving a spectral resolution of $\lambda/\delta\lambda \sim 2000$. Conditions were clear and photometric. The data were reduced following standard procedures (bias, flat, wavelength, and flux calibration) using the IRAF `twodspec` and `onedspec` packages. Observations of the standard star G191B2B (Massey & Gronwall 1990) were used to derive the response curve. Due to an observing error, we had to use a spectrum of G191B2B taken on a subsequent night through thin cirrus, so the absolute fluxes are inaccurate but the relative fluxes are sound. An approximate correction for atmospheric extinction was applied using the standard KPNO extinction curve, but we note that Kitt Peak is at a lower elevation (2100 m) than Mt. Graham (3300 m), so we are likely over-

compensating at the far blue end of the spectrum.

2.4. X-Ray Data

We combined and analyzed all *Swift* X-Ray Telescope (XRT; Burrows et al. 2005) observations obtained simultaneously with the UVOT data between 2011-10-02 and 2012-01-17. We searched for X-ray emission using a 4 pixel ($9''.6$) radius centered on the optical position of the SN and corrected for the XRT 100% encircled energy radius. The background was extracted locally using a $40''$ radius source-free aperture to account for detector and sky background, and any unresolved emission from the host.

An X-ray source is detected at the position of the SN at a 4.7σ statistical significance in the merged data (88.1 ks total exposure time). The PSF, deadtime, and vignetting corrected count rate of $(5.3 \pm 1.1) \times 10^{-4}$ counts s^{-1} corresponding to an unabsorbed (0.2–10 keV band) X-ray flux of $f_{0.2-10} = (2.3 \pm 0.5) \times 10^{-14}$ erg cm^{-2} s^{-1} and a luminosity of $L_{0.2-10} = (1.0 \pm 0.2) \times 10^{39}$ erg s^{-1} assuming a thermal plasma with $kT = 10$ keV (cf. Fransson et al. 1996; Immler et al. 2007), a Galactic foreground column density with no intrinsic absorption of $N_H = 7.8 \times 10^{19}$ cm^2 (Dickey & Lockman 1990), and a distance of 19.2 Mpc. The Swift XRT X-ray image of SN 2011ht and its host galaxy is shown in the right-hand panel of Figure 1.

Re-binning the data into two epochs with similar exposures times gives fluxes that are consistent within the statistical errors of the low photon statistics. Binning the data into an epoch ranging from 2011-11-11 to 2012-01-17 with a total exposure time 70.4 ks gives the highest S/N (5.1σ) and an X-ray flux and luminosity of $f_{0.2-10} = (3.1 \pm 0.6) \times 10^{-14}$ erg cm^{-2} s^{-1} and a luminosity of $L_{0.2-10} = (1.4 \pm 0.3) \times 10^{39}$ erg s^{-1} , respectively.

The higher flux in this late epoch and the small offset of the X-ray source from the optical position of the SN ($< 2''$), well within the XRT point-spread function ($15''$ half power diameter), confirm that the X-ray emission is from SN 2011ht, although a contamination with unresolved X-ray sources within the host galaxy cannot be excluded. Observations of previous SNe show that X-rays arise from the interaction of the outgoing SN shock with substantial amounts of circumstellar material (CSM). The bulk of the X-ray flux is produced by the reverse shock at low energies (around 1 keV) as soon as the expanding optical shell becomes optically thin for soft X-rays.

2.5. Pre-Explosion Images

The field of SN 2011ht was observed by the Galaxy Evolution Explorer (GALEX; Martin et al. 2005) as part of the All Sky Imaging Survey (ASIS) in both the near-UV (NUV; 1800–2800 Å) and far-UV (FUV; 1300–1800 Å) for a duration of 109 s on 2007-02-22. No point source is detected coincident with the position of the SN in either band (Figure 4). We measured the count rate at the SN location using a 3''8 (GALEX aperture No. 3) radius aperture in both the NUV and FUV background subtracted images and at 6 other locations that were close to the SN position and at similar isophotal brightnesses in the galaxy. Each count rate was converted into magnitudes using GALEX zero points (Morrissey et al. 2007) and an aperture correction of 0.62 mag for the NUV and 0.77 mag for the FUV. We used the standard deviation of the fluxes in these six surrounding apertures to estimate the background and its uncertainties and then set the 3σ upper limit for detecting a source at the location of the SN to be the flux at the location of the SN minus three times the standard deviation. This led to 3σ upper limits of 19.81 mag ($\nu L_\nu < 4.6 \times 10^6 L_\odot$) for the NUV and 19.66 mag ($\nu L_\nu < 7.5 \times 10^6 L_\odot$) for the FUV. The field was observed again by GALEX on 2010-04-16 for a duration of 1700 s in the NUV as part of Guest Observer program No. 61 (Figure 4: *Right*). No point source is detected coincident with the position of the SN. The 3σ upper limit derived from this image is 19.50 mag, consistent with the upper limit found from the shallower 109 s NUV ASIS data.

We also used the Sloan Digital Sky Survey (SDSS) DR8 (Aihara et al. 2011) pre-explosion images to search for a possible luminous progenitor at the position of SN 2011ht. First a *V*-band image of the field of SN 2011ht was obtained on 2011-11-01 with the Ohio State Multi-Object Spectrograph (OSMOS; Martini et al. 2011) mounted on the MDM 2.4-m telescope. The centroids of seven point sources around the SN position in the OSMOS and SDSS *g*-band images were measured, followed by a coordinate transformation between the two images using a second-order polynomial in the IRAF task `geomap`. The resulting standard deviation is 0.3 pixels in the SDSS image (0''.12). No point sources are detected in any of the SDSS *ugriz* images within the error circle of the SN position, although there is an unresolved stellar background because SN 2011ht is in a crowded environment (Figure 5). We analyzed the images with DAOPHOT (Stetson 1987) and determined a 5σ detection limit based on point sources found in regions with similar background fluxes (e.g. Li et al. 2011). The resulting 5σ upper limits on the magnitude (νL_ν) are $u = 21.9$ ($6.4 \times 10^5 L_\odot$), $g = 22.8$ ($2.1 \times 10^5 L_\odot$), $r = 22.4$ ($2.3 \times 10^5 L_\odot$), $i = 22.4$ ($1.8 \times 10^5 L_\odot$), and $z = 20.8$ ($6.7 \times 10^5 L_\odot$).

We compared these limits to blackbodies with a range of luminosities and temperatures, leading to the limits on the progenitor shown in Figure 6. These limits can then

be compared to the progenitors of known LBVs (mostly Galactic) in their “hot” state (Humphreys & Davidson 1994; de Jager 1998), yellow hypergiants (Humphreys & Davidson 1994; de Jager 1998), red supergiants (RSGs) in the LMC and SMC (Levesque et al. 2006), and the evolutionary tracks for single stars with masses of 10, 20, 40, and 80 M_{\odot} from the STARS models (Eldridge & Tout 2004) for a metallicity of $Z = 0.004$ that is consistent with the measured oxygen abundance of an HII region near SN 2011ht (see below). As expected, Figure 6 reveals that the limits are not very constraining. Many LBVs in their quiescent state (cf. Humphreys & Davidson 1994; Smith et al. 2004) are allowed, although something extreme like η -Car can be ruled out. Massive ($\gtrsim 30 M_{\odot}$) RSGs and yellow hypergiants can also be excluded.

We also retrieved the optical spectrum of UGC 5460 from SDSS DR8. The SDSS fiber was positioned on a bright H II region located 24" W and 14" N from the center of the galaxy (projected distance of ~ 2.5 kpc), and 36" W and 5" S from the location of SN 2011ht (projected distance of ~ 3.4 kpc). The spectrum is dominated by strong forbidden and recombination lines characteristic of star-forming regions, which allow us to estimate the metallicity of the gas. We use the $O3N2$ ($= \log\{([\text{O III}] \lambda 5007/\text{H}\beta)/([\text{N II}] \lambda 6583/\text{H}\alpha)\}$) ratio method described in Pettini & Pagel (2004) to estimate the oxygen abundance of the H II region. This method is fairly insensitive to reddening because it uses flux ratios of lines that are very close in wavelength. We measure the total fluxes of the emission lines using Gaussian profiles and correct for the Galactic reddening. We obtain an oxygen abundance on the $O3N2$ scale of $12 + \log(\text{O}/\text{H}) = (8.20 \pm 0.01)$ ($\sim 1/5$ Solar), where the error only reflects statistical uncertainties in the flux measurements. For this paper we assume that this is the characteristic oxygen abundance of the host galaxy and the SN region. The host galaxy properties are listed in Table 3.

3. Results

3.1. The Light Curve of SN 2011ht

In the initial UVOT observations the source is detected at 21.01 mag in the $uvw2$ filter, 19.07 mag in the $uvw1$, 17.74 mag in the u -band ³, and ~ 16.8 mag in the b and v filters. Only an upper limit was found for the $uvm2$ filter. The peak magnitudes are ~ 13.4 , ~ 13.3 , ~ 14.4 , and ~ 14.4 in the UV ($uvw2$, $uvm2$, $uvw1$), u , b , and v filters, respectively.

³Note that the effective wavelength of the UVOT u -band filter is bluer than when used on the ground because it is unaffected by atmospheric absorption.

The peak occurred ~ 43 days after discovery in the UV and u bands, and after ~ 55 days in the b and v bands. The initial rise in the light curves (the first 20 days) is quite sharp, particularly in the UV ($\Delta uvw2 = 0.32$, $\Delta uvm2 = 0.32$, $\Delta uvw1 = 0.23$, $\Delta u = 0.18$, $\Delta b = 0.11$, and $\Delta v = 0.07 \text{ mag day}^{-1}$), followed by a slower rise to peak (over the next ~ 20 – 30 days; $\Delta uvw2 = 0.062$, $\Delta uvm2 = 0.064$, $\Delta uvw1 = 0.063$, $\Delta u = 0.045$, $\Delta b = 0.023$, and $\Delta v = 0.017 \text{ mag day}^{-1}$). The initial ASAS-SN observations began ~ 23 days after discovery. The rise in the light curve is $0.05 \text{ mag day}^{-1}$, consistent with the average of the 0.07 and 0.017 UVOT Δv rise times. After peak, all photometric bands are observed to fade, although the UV fades more rapidly ($\Delta uvw2 = 0.09$, $\Delta uvm2 = 0.09$, $\Delta uvw1 = 0.07$, $\Delta u = 0.05$, $\Delta b = 0.03$, and $\Delta v = 0.02 \text{ mag day}^{-1}$). The $\Delta_\lambda(15)$ for the UV and ubv bands is ~ 0.2 and 0.04 , respectively.

The color evolution is peculiar because it evolves from red to blue at early times (Figure 2: *Bottom*), followed by a more normal, slow reddening after the peak. This is best summarized by examining the evolution of the luminosity and temperature, which we can approximate well because of the wavelength coverage provided by the UVOT. We fit the spectral energy distributions (SEDs) as blackbodies, allowing for Galactic extinction ($E(B-V)=0.01$; Schlegel et al. 1998) as well as additional extinction in the host with a range of reddening laws (MW, LMC, SMC)⁴. Our best fit host reddening value is zero, but values up to ~ 0.2 are consistent with the data. If we only fit the peak, where the S/N is best, we obtain values of $E(B-V)=0.062$ (MW) and 0.041 (SMC/LMC). We adopt the $E(B-V)=0.062$ MW model for our standard reddening estimate. In Figure 7 we compare a blackbody with $E(B-V)=0$, 0.041 , and 0.062 to the combined ARC/DIS and UVOT/uvg (Epoch 2) spectrum. The blackbody approximates the SED reasonably well in the optical, but the fluxes overestimate somewhat the UV due to line blanketing.

We also estimate a pseudo-bolometric luminosity. We use count rate to flux conversions for the best fit blackbody temperatures interpolated from blackbody values in Brown et al. (2010), and then arrive at an average monochromatic flux density for each filter. The flux density is then integrated over the filter bandpass using trapezoidal integration. Figure 8 shows that these two estimates of the luminosity agree reasonably well, with the agreement improving as the temperature increases and there is proportionately less unobserved optical/near-IR emission. The bolometric light curve peaks at $\sim 10^9 L_\odot$, roughly ~ 43 days after discovery. The total energy emitted by the SN in the first 112 days is $\sim 2.5 \times 10^{49}$ ergs. For comparison purposes, this is $\sim 100\times$ greater-than the energy in the eruption of the

⁴The UVOT $uvw2$ and $uvw1$ filters suffer from a red leak that can lead to complications in the analysis of red spectra (Brown et al. 2010; Milne et al. 2010). The early spectra of SN 2011ht are very blue, and we account for the red leaks in the filter response functions used for the model SEDs.

2008 N300 transient (Humphreys et al. 2011) and $\sim 100\times$ less-than the radiated output of SN 2006gy (Smith et al. 2007).

Figure 9 shows the evolution of the blackbody fits in temperature (T_{BB}), radius (R_{BB}), and luminosity (L_{BB}) along with the fit residuals. The fits are worse at early times, but we see a general trend that as the temperature increases the luminosity increases and the black body radius shrinks and then remains fairly constant until peak. After peak, T_{BB} and L_{BB} begin declining, while R_{BB} begins increasing. The estimates of T_{BB} , R_{BB} , and L_{BB} for each epoch are reported in Table 4.

3.2. The Spectra of SN 2011ht

A close examination of the UVOT/uvgr spectra (Figure 3) reveals absorption lines of Fe II and potential lines of Si II, Si III, Ni II, and N III. The UV spectrum below 1900 Å shows significant absorption features which differ between the two spectra taken 11 days apart. The most likely explanation is a combination of noise in the early spectrum and physical changes in the state and velocity of the circumstellar matter. Only the longer exposure of the later spectrum can be trusted below 1900 Å. The spectra also show broadened hydrogen lines of H β , H γ , and H δ .

The UV is dominated by lines of Fe II, most notably the UV1, UV2 and UV62 multiplets. A comparison with the SN 1998S spectrum from Bowen et al. (2000) reveals that several sets of absorption lines match the SN 2011ht lines, namely Mg II ($\sim \lambda 2800$) and Fe II ($\sim \lambda 2400$, $\lambda 2586$, and $\lambda 2612$; Figure 10). An 11 Å shift of the UVOT spectrum (which is within the wavelength accuracy of the instrument) was applied based on the line identifications, so it is possible that the overall blueshift seen in the optical is masked.

At $\lambda 1751$ Å there is a possible resonance line of Ni II, but this is more likely the N III ($\lambda 1750$ Å) resonance line that is broadened by a velocity of ~ 1880 km s $^{-1}$. The Si III $\lambda 1842$, and $\lambda 2562$ lines are not resonance lines, but are probably the result of a cascade from Si IV. The line broadening of the two Si III lines indicates velocities of 1220 and 1474 km s $^{-1}$, respectively. We attribute the line found at $\lambda 1813$ Å to $\lambda 1808$, $\lambda 1816$, $\lambda 1817$ triplet of Si II. The C III] ($\lambda 1909$ Å) line is seen at ~ 1904 Å. The Mg II resonance lines at $\lambda 2797$ and $\lambda 2802$ Å are present, while we also see the Mg II ($\lambda 2930$ Å) line whose lower level is the upper level of the $\lambda 2802$ Å line. Similar to the Si III lines this could be due to recombination of the Mg III levels or due to high temperature collisional excitation. The width of the UV lines is difficult to determine since there are so many faint Fe II lines confusing the measurements. A FWHM between 25–33 Å is our best estimate, which equates to a velocity of about 1670 km s $^{-1}$.

The early optical spectra are dominated by strong asymmetric (the red side having greater flux) Balmer emission lines with narrow peaks, very broad wings, and P-Cygni profiles. Using the MODS1 spectrum we have measured velocities with respect to the various rest frame peak emission and absorption lines (Table 5). From the H α P-Cygni profile, we measure blueshifted velocities (with respect to the velocity of the galaxy) of 261 and 778 km s⁻¹ in emission and absorption, respectively. We also measure the width of the narrow H α line to be FWHM_{H α -Line} \simeq 600 km s⁻¹ while the broad wings are FWHM_{H α -Wing} \simeq 4200 km s⁻¹. The H α profile remains fairly consistent over the five epochs (see Figure 11). The velocity in absorption decreases in the higher Balmer lines (see Table 5), and the absorption lines become stronger as the emission weakens (Figure 12). H η has no obvious emission altering the absorption profile, so we measure the absorption velocity to be 646 km s⁻¹. Paschen lines are easily identified on the red end of the spectrum. They show weak emission combined with blue shifted absorption.

There are two very strong He I emission lines (λ 7065 and λ 5876), both of which show very broad wings. The λ 5876 line has an absorption feature similar to the hydrogen lines, but the absorption is absent from the λ 7065 line (Figure 13). The other He I lines are weak. Normally He I (λ 6678) is a very strong line, but it lies on the red wing of H α and is difficult to analyze. The emission and absorption in the other He I lines (λ 5015, λ 4921, λ 4471, λ 4026, and λ 3819) are weaker, with the latter two lines having the weakest emission. Redward of H γ is a peculiar continuum where the He I (λ 4471) line weakly appears in emission. This could be the result of Thomson scattering.

The O I absorption triplet at λ 7774 (λ 7772.0, λ 7774.2, and λ 7775.4) is strong and has a velocity of 618 km s⁻¹, similar to the H and He I absorption features. There are also three weak absorption lines between 3900 and 4000 Å. The line measured at 3939.6 Å is most likely Ca II K with a velocity of \sim 650 km s⁻¹.

In the last spectrum taken with the HET/LRS, the strong, broad He I emission lines at λ 5876 and λ 7065 have disappeared. The other He I lines (λ 4921 and λ 5015) are still present with weak P-Cygni profiles. Several Fe II lines have appeared in both absorption and emission. The strong absorption and P-Cygni emission is Fe II (λ 4924 multiplet 42) with the next absorption line probably being Fe II (42) at λ 5169. There are four Fe II absorption/emission lines from 5200–5340 Å all from multiplet 49. The O I absorption is still present and strong.

4. Discussion

Some of the properties of SN 2011ht are similar to SN impostors (e.g. the emission line structures), while others are comparable to true SNe IIn (e.g. the luminosity) – SN 2011ht has the luminosity of a normal core-collapse SNe (see Figure 14), but the spectrum of a dense wind (see Figure 15). The spectrum originally showed hydrogen and the Ca II triplet in emission with P-Cygni profiles, as well as narrow absorption lines of Fe II (Pastorello et al. 2011), typical of LBVs at maximum and during giant eruptions. The steep, blue continuum, strong UV flux, and the properties of the He I lines are not characteristic of dense winds. The UV decay slope of the SN 2011ht light curve is reminiscent of SN 2007pk (Pritchard et al. 2012).

The broad asymmetric (to the red) wings in SN 2011ht are suggestive of Thomson scattering. The SN impostors, SNe 1999bw and 2001ac, showed strong, narrow Balmer lines ($\text{FWHM}_{\text{H}\alpha\text{-Lines}} \simeq 630$ and 290 km s^{-1} , respectively) characteristic of LBVs, with broad wings ($\text{FWHM}_{\text{H}\alpha\text{-Wings}} \simeq 6000$ and 3000 km s^{-1} , respectively). The cause of these wings is not clear, but they have been attributed to either electron scattering, fast moving ejecta, or a combination of both (Smith et al. 2011a). The cause of the broad wings in SNe is not always clear either. For SN 1998S, the broad component has been attributed both to the ejecta (Leonard et al. 2000) and to scattering on thermal electrons (Chugai 2001). In SN 1999W, Chugai et al. (2004) attributed the broad wings to a combination of cool shocked gas and Thomson scattering, while Dessart et al. (2009) argued they were primarily the result of electron scattering in the ejecta. Even with detailed models it can be difficult to reach a conclusive interpretation. Further complicating this picture is that some SNe IIn initially reveal a Thomson scattering profile but evolve to a shocked profile (Smith et al. 2012).

If we suppose both the presence of Thomson scattering in a pre-existing circumstellar medium (CSM) in order to produce the line structures, and that the transient is a true SN based on its energetics, then we would expect a shock wave to be propagating through the CSM with observable effects. Significantly modifying the line structures requires $\tau_T \simeq 1$ on the scale of the apparent photosphere (Figure 9), and we use this to normalize the model by

$$\dot{M} = \frac{4\pi v_w R_{in} \tau_T}{\kappa_T} \simeq 0.02 \tau_T \left(\frac{v_w}{600 \text{ km/s}} \right) \left(\frac{R_{in}}{5 \times 10^{14} \text{ cm}} \right) \left(\frac{\Delta R}{R_{out}} \right) M_{\odot} \text{ year}^{-1}.$$

where the Thomson opacity is $\kappa_T \simeq 0.34$ and we identify the absorption feature of the spectra with the wind speed (v_w). The shell extends from R_{in} to R_{out} with a thickness $\Delta R = R_{out} - R_{in}$. The term $\Delta R/R_{out} \rightarrow 1$ for a thick shell. Producing significant levels of Thomson scattering on these large scales requires a very dense wind, similar to that of an LBV in eruption (Kochanek 2011a). We can then estimate the H α luminosity assuming it

is due to recombination outside radius R_{in} (and ignoring R_{out}) as

$$L_{H\alpha} \simeq \frac{4\pi E_{H\beta} \alpha_{H\beta} R_{in} \tau_T^2}{\mu^2 m_p^2 \kappa_T^2} \simeq 4 \times 10^6 \left(\frac{R_{in}}{5 \times 10^{14} \text{ cm}} \right) \tau_T^2 L_{\odot} \quad (1)$$

where $E_{H\alpha} = 1.9 \text{ eV}$, $\alpha_{H\alpha} \simeq 10^{-13} \text{ cm}^3/\text{s}$ is the $H\alpha$ rate, and $\mu \simeq 0.6$ is the mean molecular weight. For the estimated $H\alpha$ line flux of $5 \times 10^{-13} \text{ ergs cm}^{-2} \text{ s}^{-1}$ ($6 \times 10^6 L_{\odot}$) in the MODS spectrum, the line formation radius will be consistent with the photometric radius for $\tau_T \simeq 1$, roughly as needed to broaden the lines with Thomson scattering.

A shock propagating through such a medium releases a significant amount of energy, with a shock luminosity of

$$L_s \simeq \frac{\dot{M} v_s^3}{2v_w} = \frac{2\pi \tau_T R_{in} v_s^3}{\kappa_T} \left(\frac{\Delta R}{R_{out}} \right) \simeq 2 \times 10^7 \tau_T \left(\frac{v_s}{2000 \text{ km/s}} \right)^3 \left(\frac{R_{in}}{4 \times 10^{14} \text{ cm}} \right) \left(\frac{\Delta R}{R_{out}} \right) L_{\odot}$$

(e.g. Miller et al. 2010), where we have set the shock velocity to 2000 km s^{-1} , an intermediate velocity between the narrow and broad components. While this energy can be lost to re-accelerating the expansion of the flow, on these physical scales it will tend to be radiated. The natural shock temperature is $kT_s \simeq 5 \text{ keV}$. If the optical depth of the wind is low, the X-rays from the shock cannot be thermalized and simply escape. Averaging over the X-ray epochs from 11 November to 17 January (days 43-110) gives a detection with $L_X = (3.9 \pm 0.8) \times 10^5 L_{\odot}$. These can be reconciled by having a low optical depth, $\tau_T \simeq 0.02$ corresponding to a mass loss rate of a few $10^{-4} M_{\odot} \text{ year}^{-1}$. A possible difficulty is that at the low shock densities implied by this optical depth, one would be directly observing the shock and would expect to see the characteristic emission lines associated with fast shocks (e.g. the late time spectra of SN 1980K; Fesen & Matonick 1994), although they would be heavily diluted by the large ratio between the shock and photospheric luminosities.

The alternative is to make the medium dense enough so that the X-rays are absorbed before they escape (see the recent discussion in Chevalier & Irwin 2012). At the densities and temperatures we expect to see in the shell, the material is likely to be incompletely ionized, which means that the optical opacity (dominated by electron scattering) will be low compared to the X-ray opacity (e.g. Figure 16). In these conditions, $\tau_{X\text{-rays}} \gg \tau_T$ and, if we require $\tau_T \approx 1$ to fit the line profiles, the high X-ray optical depth will be sufficient to severely limit the softer X-rays to which *Swift* is most sensitive. There is an upper bound of $\tau_T \lesssim 100$ where L_s begins to exceed the bolometric luminosity of the transient. If we follow the argument of Chevalier & Irwin (2012) and try to produce all the luminosity from an embedded shock, the energy available to heat the medium is $L_s \Delta R \tau / c$, where $t_d \simeq 3 \Delta R \tau / c$ is how long it takes the energy to escape. We equate this with the radiative energy $4\pi \Delta R R_{in}^2 a T^4$ to estimate a

temperature

$$T = \left(\frac{3L_s\tau}{16\pi R_{in}^2\sigma} \right)^{1/4} \simeq 11000 \left(\frac{L_s}{10^9 L_\odot} \right)^{1/4} \left(\frac{5 \times 10^{14} \text{ cm}}{R_{in}} \right)^{1/2} \tau^{1/4} \text{ K}. \quad (2)$$

Thermalizing the shock photons to limit the X-ray transmittance places constraints on the ionization state of the atoms. To explain the line profiles, we require $\tau_T \sim 1$. But the optical depth cannot be too high, or the photon diffusion time becomes too long and the shock breaks out before the radiation. This also implies that $\tau_T \lesssim 100$. The mass associated with the shell is then

$$M = 4\pi \frac{\tau_T}{\kappa_T} R_{in} R_{out} \simeq 0.01 \tau_T \left(\frac{R_{in}}{5 \times 10^{14} \text{ cm}} \right) \left(\frac{R_{out}}{10^{15} \text{ cm}} \right) M_\odot \quad (3)$$

where we have used $\kappa_T = 0.34 \text{ cm}^2 \text{ g}^{-1}$ for a largely ionized medium, but it can be lower if the H/He are able to partially recombine (see Figure 16). These masses and mass loss rates in these high luminosity models are typical of other Type IIn SNe (e.g. Kiewe et al. 2010) and are in the range of LBVs in eruption (e.g. Kochanek 2011b).

There is one additional attractive feature of surrounding an explosive transient with a discontinuous shell of material. Namely, it might be able to explain the large photospheric radius and low temperature of the first few epochs (see Figure 9). When the shock breaks out of the surface of the star, it produces a luminosity UV/X-ray spike in excess of $10^{40} \text{ ergs s}^{-1}$ in a brief burst. The duration depends on the structure of the star, wind profile and the photon energy, but the bulk of the breakout emission occurs well within 10,000 s (e.g. Fryer et al. 2009; Frey et al. 2012). In a shell geometry, this short radiation spike rapidly crosses to the shell and then photoionizes it before escaping. But if the radiation interacts in the shell, it is spread over the diffusion time $t_d \simeq 3\tau\Delta R/c \simeq \tau(\Delta R/10^{15} \text{ cm}) \text{ days}$, which is relatively well-matched to the duration and apparent photospheric scales of the initial phase. The problem is that the required luminosity is at the high end of what we might expect from shock breakout. This can be explored further once the nature of this transient is fully understood.

5. Conclusions

SN 2011ht shows a series of curious behaviors. It has a spectrum broadly resembling a dense stellar wind but the overall luminosity and energetics of a true core-collapse SN. It appeared to have a very large, cool photosphere initially, which then shrinks to roughly a constant before starting to slowly expand. The apparent temperature rises dramatically

from ~ 5000 K to almost 14,000 K before starting to decline. At early times there seems to be no X-ray emission, and then it is detected only to probably fade again.

Clearly continued photometric and spectroscopic monitoring of this system is necessary. Combining a shock from an explosive transient with a dense stellar wind has the prospect of explaining some of the peculiarities, but such shocks have to eventually emerge at low optical depths which should dramatically change the spectroscopic and X-ray properties as the transient evolves.

JLP acknowledges support from NASA through Hubble Fellowship Grant HF-51261.01-A awarded by STScI, which is operated by AURA, Inc. for NASA, under contract NAS 5-2655. CSK, BJS, DMS and KZS are supported by NSF grant AST-0908816. KZS and RS are also supported by NSF grant AST-1108687. JFB was supported by NSF grant PHY-1101216. We gratefully acknowledge the contributions from members of the *Swift* UVOT team at the Pennsylvania State University (PSU), University College London/Mullard Space Science Laboratory (MSSL), and NASA/Goddard Space Flight Center. This work is sponsored at PSU by NASA contract NAS5-00136 and at MSSL by funding from the Science and Technology Facilities Council (STFC) and the UK Space Agency. The ASAS-SN commissioning observations were only possible due to help and support of the Las Cumbres Observatory, especially W. Rosing, E. Hawkins, R. Ross, M. Elphick, D. Mullins and Z. Walker. We thank R. McMillan and G. Bakos for obtaining a spectrum with the APO 3.5-m telescope, and the APO director S. Hawley for granting DD time for this observation. This paper used data taken with the LBT/MODS1 spectrographs built with funding from NSF grant AST-9987045 and the NSF Telescope System Instrumentation Program (TSIP), with additional funds from the Ohio Board of Regents and the Ohio State University Office of Research. The Hobby Eberly Telescope (HET) is a joint project of the University of Texas at Austin, PSU, Stanford University, Ludwig-Maximilians-Universität München, and Georg-August-Universität Göttingen. The HET is named in honor of its principal benefactors, William P. Hobby and Robert E. Eberly. The Marcario Low Resolution Spectrograph (LRS) is named for Mike Marcario of High Lonesome Optics who fabricated several optics for the instrument but died before its completion. The LRS is a joint project of the HET partnership and the Instituto de Astronomia de la Universidad Nacional Autónoma de México. Based in part on observations made with the Large Binocular Telescope. The LBT is an international collaboration among institutions in the United States, Italy and Germany. The LBT Corporation partners are: the University of Arizona on behalf of the Arizona university system; the Istituto Nazionale di Astrofisica, Italy; the LBT Beteiligungsgesellschaft, Germany, representing the Max Planck Society, the Astrophysical Institute Potsdam, and Heidelberg University; the Ohio State University; and the Research Corporation, on behalf

of the University of Notre Dame, University of Minnesota and This research has made use of the NASA/IPAC Extragalactic Database (NED) which is operated by the Jet Propulsion Laboratory, California Institute of Technology, under contract with the National Aeronautics and Space Administration.

Facilities: Swift (UVOT), ARC (DIS), HET (LRS), LBT (MODS1)

REFERENCES

- Aihara, H., et al. 2011, ApJS, 193, 29
- Bloom, J. S., Starr, D. L., Blake, C. H., Strutskie, M. F., & Falco, E. E. 2006, ASP Conf. Ser., 351, 751
- Boles, T., Pastorello, A., Stanishev, V., Smartt, S. J., Fraser, M., & Lindborg, M. 2011, CBET 2851
- Botticella, M. T., et al. 2009, MNRAS, 398, 1041
- Bowen, D. V., Roth, K. C., Meyer, D. M., & Blades, J. C. 2000, ApJ, 536, 225
- Breeveld, A. A., et al. 2010, MNRAS, 406, 1687
- Brown, P. J. 2009, PhD Dissertation (Penn State University), 14
- Brown, P. J., et al. 2009, AJ, 137, 4517
- Brown, P. J., et al. 2010, ApJ, 721, 1608
- Burrows, D. N., et al. 2005, Space Sci. Rev., 120, 165
- Chandra, P., et al. 2009, ApJ, 690, 1839
- Chatzopoulos, E., et al. 2011, ApJ, 729, 143
- Chevalier, R. A., & Irwin, C. M. 2012, arXiv:1201.5581
- Chugai, N. N. 1990, Soviet Ast., 16, 457
- Chugai, N. N. 2001, MNRAS, 326, 1448
- Chugai, N. N., et al. 2004, MNRAS, 352, 1213
- Cooke, J. 2008, ApJ, 677, 137

- Cooke, J., Sullivan, M., Barton, E. J., Bullock, J. S., Carlberg, R. G., Gal-Yam, A., & Tollerud, E. 2009, *Nature*, 460, 237
- Corwin H. G., Buta R. J., & de Vaucouleurs G. 1994, *AJ*, 108, 2128
- Davidson, K., & Humphreys, R. M. 1997, *ARA&A*, 35, 1
- Dessart, L., Hillier, D. J., Gezari, S., Basa, S., Matheson, T. 2009, *MNRAS*, 394, 21
- de Jager, C. 1998, *A&A Rev.*, 8, 145
- de Vaucouleurs G., de Vaucouleurs A., Corwin H. G., Buta R. J., Paturel G., & Fouque P. 1991, *Third Reference Catalogue of Bright Galaxies* (Springer-Verlag: New York)
- Dickey, J. M., & Lockman, F. J. 1990, *ARA&A*, 28, 215
- Draine, B. T., & Woods, D. T. 1991, *ApJ*, 383, 621
- Drake, A. J., et al. 2009, *ApJ*, 696, 870
- Drake, A. J., et al. 2010, *ApJ*, 718, 127
- Drake, A. J., et al. 2011, *ApJ*, 735, 106
- Eldridge, J. J. & Tout, C. A. 2004, *MNRAS*, 348, 201
- Fesen, R. A., & Matonick, D. M. 1994, *ApJ*, 428, 157
- Filippenko, A. V., Li, W. D., Treffers, R. R., & Modjaz, M. 2001, *ASP Conf. Ser.*, 246, 121
- Foley, R. J., Berger, E., Fox, O., Levesque, E. M., Challis, P. J., Ivans, I. I., Rhoads, J. E., & Soderberg, A. M. 2011, *ApJ*, 732, 32
- Fransson, C., Lundqvist, P., & Chevalier, R. A. 1996, *ApJ*, 461, 993
- Frey, L. et. al. 2012, in preparation
- Fryer, C. L., Rockefeller, G., & Young, P. A. 2006, *ApJ*, 647, 1269
- Fryer, C. L., et al. 2009, *ApJ*, 707, 193
- Fukugita, M., Ichikawa, T., Gunn, J. E., Doi, M., Shimasaku, K., Schneider, D. P. 1996, *AJ*, 111, 1748
- Gal-Yam, A., et al. 2007, *ApJ*, 656, 372

- Gehrels, N., et al. 2004, ApJ, 611, 1005
- Hamuy, M., et al. 2003, Nature, 424, 651
- Hamuy, M., et al. 2006, PASP, 118, 2
- Hill, G. J., Nicklas, H. E., MacQueen, P. J., Tejada, C., Cobos Duenas, F. J., & Mitsch, W. 1998, Proc. SPIE, 3355, 375
- Humphreys, R. M., & Davidson, K. 1994, PASP, 106, 1025
- Humphreys, R. M., et al. 2011, ApJ, 743, 118
- Immler, S., et al. 2007, ApJ, 664, 435
- Kiewe, M., et al. 2010, ApJ, submitted (arXiv:1010.2689)
- Kochanek, C. S. 2011a, ApJ, 743, 73
- Kochanek, C. S. 2011b, ApJ, 741, 37
- Kochanek, C. S., Szczygiel, D. M., & Stanek, K. Z. 2011, ApJ, submitted (arXiv:1202.0281)
- Law, N. M., et al. 2009, PASP, 121, 1395
- Lentz, E. J., et al. 2001, ApJ, 547, 406
- Leonard, D. C., Filippenko, A. V., Barth, A. J., & Matheson, T. 2000, ApJ, 536, 239
- Levesque, E. M., Massey, P., Olsen, K. A. G., Plez, B., Meynet, G., Maeder, A. 2006, ApJ, 645, 1102
- Li, C., et al. 2011, MNRAS, *in press*
- Liu, Q. -Z., Hu, J. Y., Hang, H. R., Qiu, Y. L., Zhu, Z. -X., & Qiao, Q. -Y. 2000, A&A, 144, 219
- Magee, N. H., et al. 1995, ASP Conf. Ser., 78
- Martin, D. C., et al. 2005, ApJ, 619, 59
- Martini, P., et al. 2011, PASP, 123, 187
- Massey, P., & Gronwall, C. 1990, ApJ, 358, 344
- Miller, A. A., et al. 2010, MNRAS, 404, 305

- Milne, P. A., et al. 2010, *ApJ*, 721, 1627
- Morrissey, P., et al. 2007, *ApJS*, 173, 682
- Ofek, E. O., et al. 2010, *ApJ*, 724, 1396
- Panagia, N. 2003, *Lect. Notes Phys.*, 598, 113
- Pastorello, A., et al. 2002, *MNRAS*, 333, 27
- Pastorello, A., Aretxaga, I., Zampieri, L., Mucciarelli, P., & Benetti, S. 2005, *ASP Conf. Ser.*, 342, 285
- Pastorello, A., Stanishev, V., Smartt, S. J., & Fraser, M. 2011, *CBET* 2851
- Pettini, M., & Pagel, B. E. J. 2004, *MNRAS*, 348, 59
- Pogge, R. W., et al. 2010, *Proc. SPIE*, 7735, 9
- Poole, T. S., et al. 2008, *MNRAS*, 383, 627
- Prieto, J. L., McMillian, R., & Bakos, G. 2011b, *CBET* 2903
- Prieto, J. L., et al. 2007, *arXiv:0706.4088*
- Prieto, J. L., et al. 2008, *ApJ*, 681, 9
- Prieto, J. L., et al. 2011a, *ATEL*, 3749
- Pritchard, T. A., et al. 2012, *ApJ*, submitted
- Quimby, R. M. 2006, PhD Dissertation (University of Texas at Austin)
- Ramsey, L. W., et al. 1998, *Proc. SPIE*, 3352, 34
- Rau, A., et al. 2009, *PASP*, 121, 1334
- Roming, P., Pritchard, T., & Brown, P. 2011, *ATEL*, 3690
- Roming, P. W. A., et al. 2000, *Proc. SPIE*, 4140, 76
- Roming, P. W. A., et al. 2004, *Proc. SPIE*, 5165, 262
- Roming, P. W. A., et al. 2005, *Space Sci. Rev.*, 120, 95
- Roming, P. W. A., et al. 2009, *ApJ*, 690, 163

- Schlegel, D. J., Finkbeiner, D. P., & Davis, M. 1998, *ApJ*, 500, 525
- Schlegel, E. M. 1990, *MNRAS*, 244, 269
- Smith, N., & Frew, D. J. 2011, *MNRAS*, 415, 2009
- Smith, N., Vink, J. S., & de Koter, A. 2004, *ApJ*, 615, 2004
- Smith, N., et al. 2007, *ApJ*, 666, 1116
- Smith, N., et al. 2008, *ApJ*, 686, 485
- Smith, N., et al. 2009, *ApJ*, 697, L49
- Smith, N., Chornock, R., Silverman, J. M., Filippenko, A. V., & Foley, R. J. 2010a, *ApJ*, 709, 856
- Smith, N., et al. 2010b, *AJ*, 139, 1451
- Smith, N., Li, W., Silverman, J. M., Ganeshalingam, M., & Filippenko, A. V. 2011a, *MNRAS*, 415, 773
- Smith, N., et al. 2011b, *ApJ*, 723, 63
- Smith, N., et al. 2012, *AJ*, 143, 17
- Sollerman, J., Cumming, R. J., & Lundqvist, P. 1998, *ApJ*, 493, 933
- Stetson, P. B. 1987, *PASP*, 99, 191
- Szczygieł, D. M., Prieto, J. L., Kochanek, C. S., Stanek, K. Z. Thompson, T. A., Beacom, J. F., Garnavich, P. M., & Woodward, C. E. 2012, *ApJ*, submitted (arXiv:1202.0279)
- Thompson, T. A., Prieto, J. L., Stanek, K. Z., Kistler, M. D., Beacom, J. F., Kochanek, C. S. 2009, *ApJ*, 705, 1364
- Van Dyk, S. D., Peng, C. Y., King, J. Y., Filippenko, A. V., Treffers, R. R., Li, W., & Richmond, M. W. 2000, *PASP*, 112, 1532

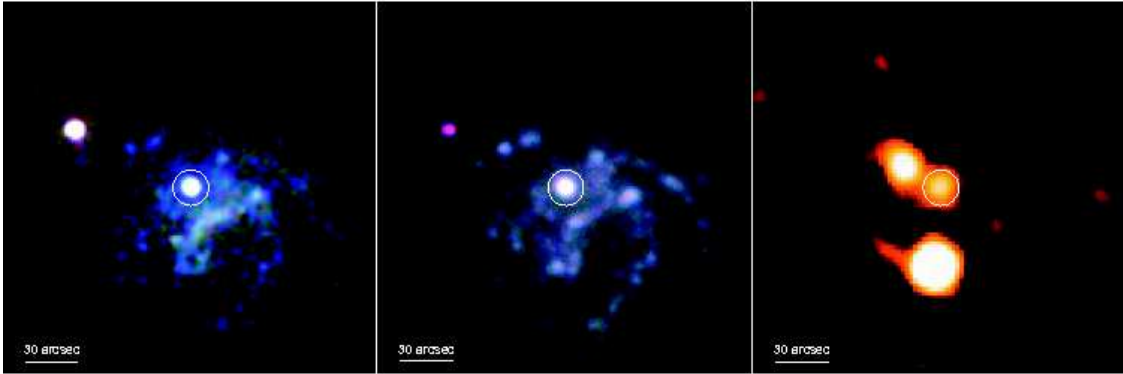


Fig. 1.— *Swift* UVOT optical (*left*), UVOT UV (*middle*), and XRT X-ray (*right*) images of SN 2011ht and its host galaxy UGC 5460. *Left*: The optical image was constructed from the UVOT *v* (64 s; red), *b* (64 s; green), and *u* (64 s; blue) filters obtained on 2011-11-02. *Middle*: The UV image was constructed from the UVOT *uvw1* (20 s; red), *uvw2* (20 s; green), and *uvw3* (33 s; blue) filters obtained on 2011-11-02. *Right*: The X-ray image (0.2–10 keV) was constructed from merged XRT data obtained between 2011-10-02 and 2012-01-17 (88.1 ks exposure time). All images are smoothed with a 3 pixels FWHM Gaussian. The position of SN 2011ht is indicated by a circle with a radius of $10''$.

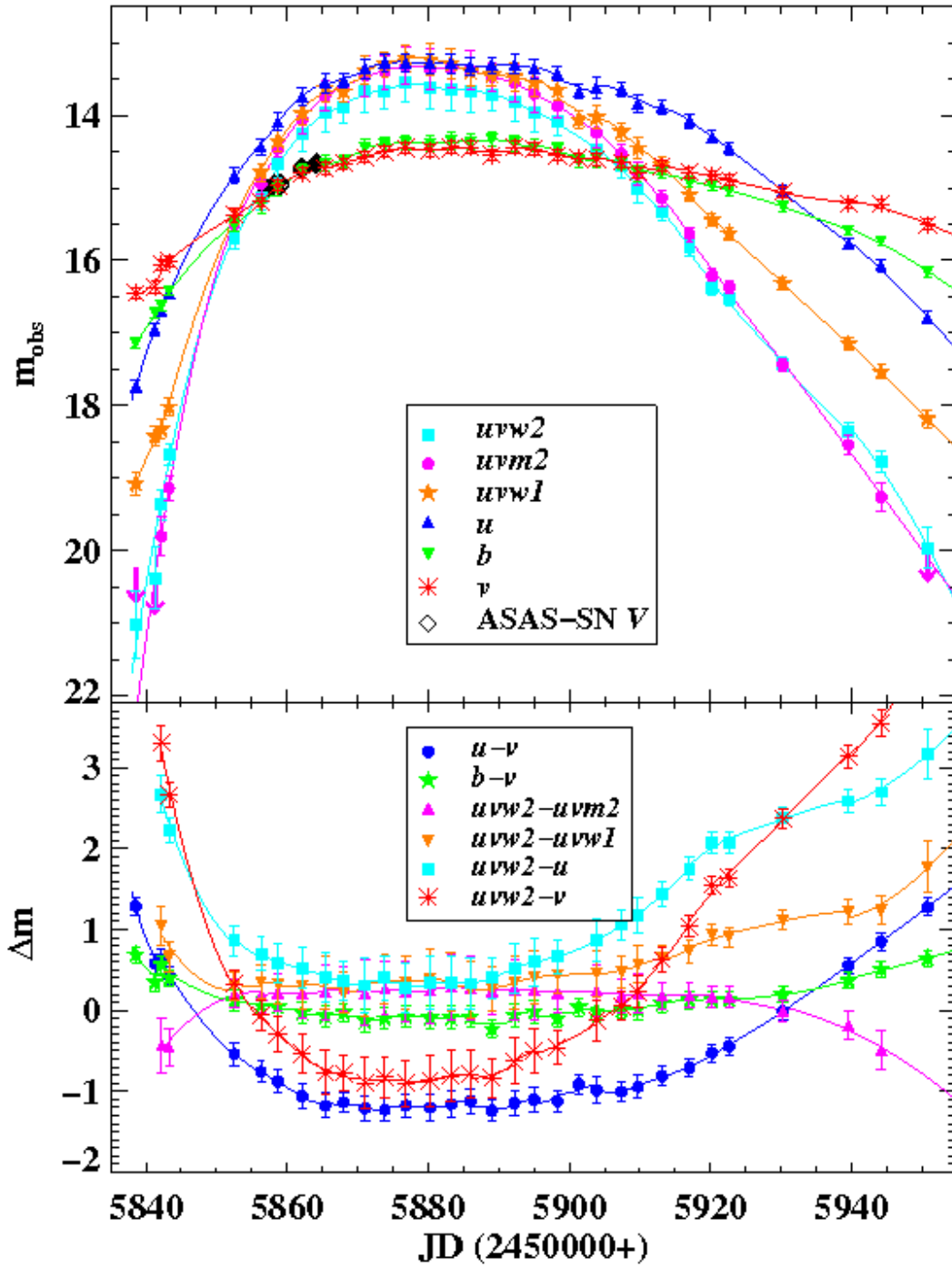


Fig. 2.— *Top:* *Swift* UVOT and ASAS-SN light curves of SN 2011ht. *Bottom:* Color evolution of SN 2011ht.

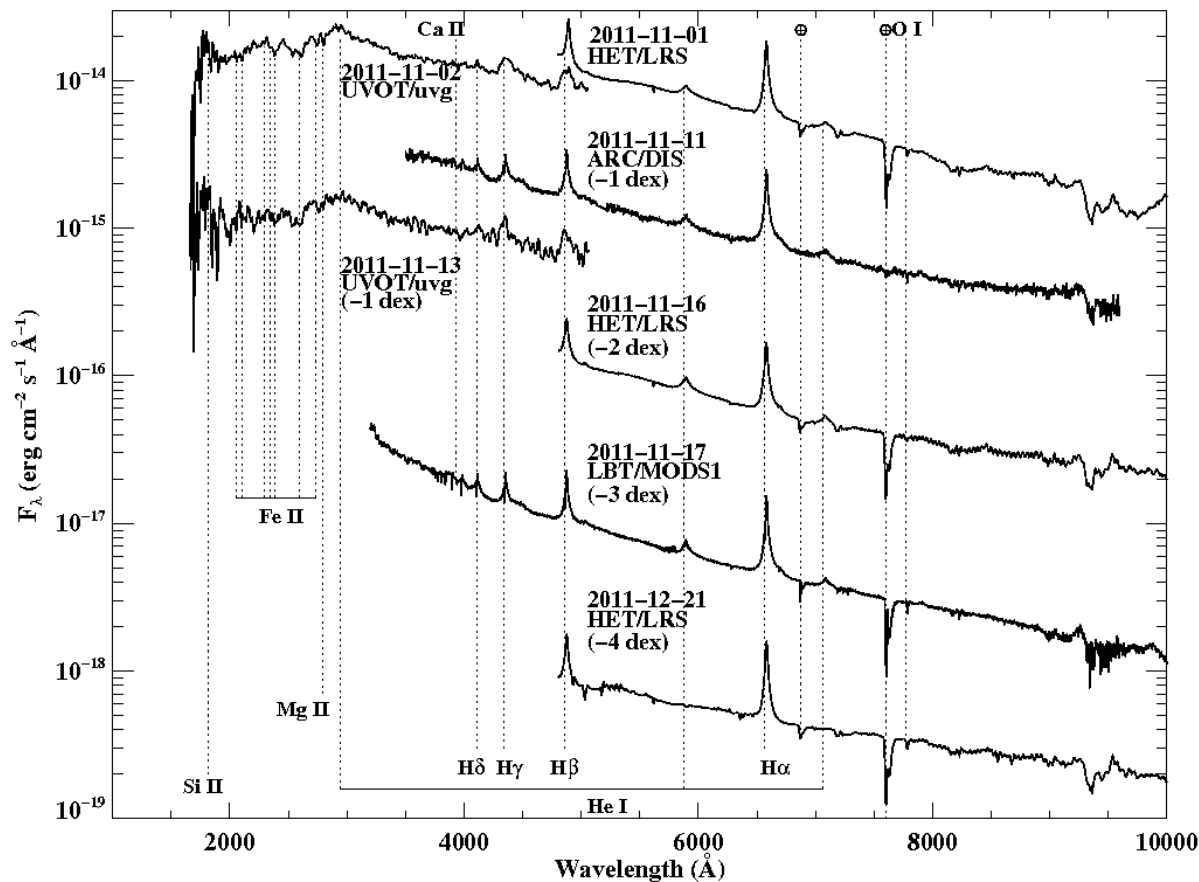


Fig. 3.— HET/LRS, UVOT/uvg, ARC/DIS, and LBT/MODS1 spectra of SN 2011ht. Prominent absorption and emission lines, as well as telluric bands, are indicated. The wavelengths have been corrected to the rest frame using $v_{\text{helio}} = 1093 \text{ km s}^{-1}$. The spectra have not been corrected for line-of-sight extinction.

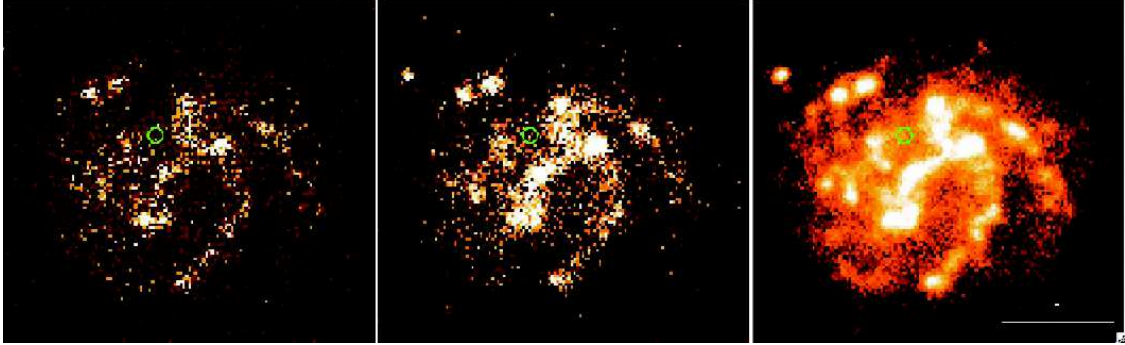


Fig. 4.— GALEX FUV (*left*) and NUV (*middle*) 109 s images of UGC 5460 taken on 2007-02-22. GALEX NUV (*right*) 1700 s image of UGC 5460 taken on 2010-04-16. The SN position is indicated by the $5''$ circles.

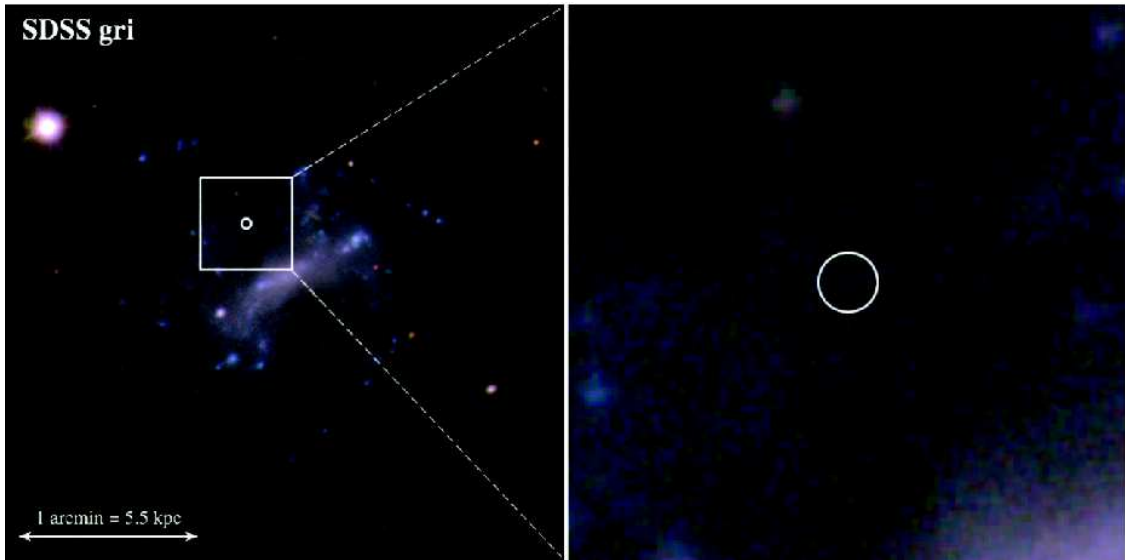


Fig. 5.— Pre-explosion SDSS *gri* images of UGC 5460. *Left*: $3' \times 3'$ image centered on the host galaxy showing the SN location with respect to the spiral arms. *Right*: $30'' \times 30''$ region around the SN showing the environment. The circle at the position of the SN has a radius of $0''.6$, which is $5 \times$ the uncertainty in the SN position.

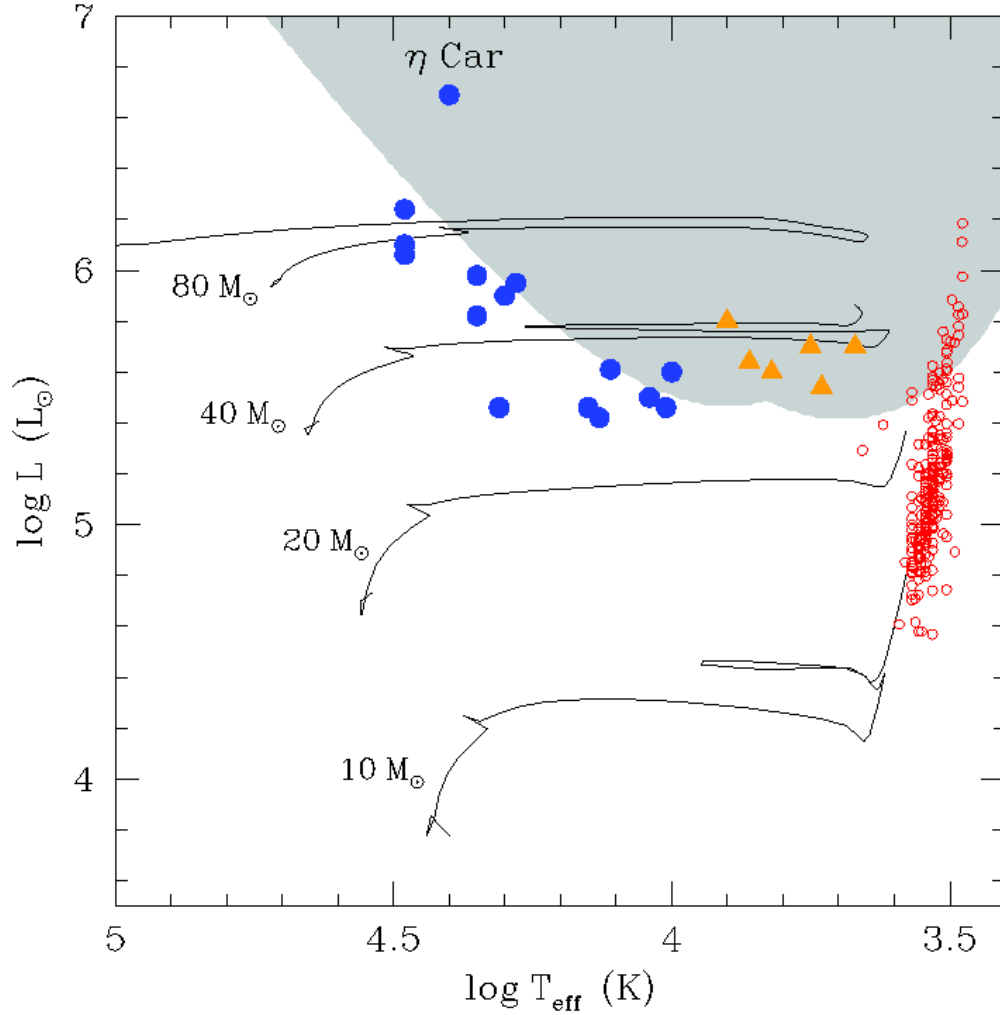


Fig. 6.— Constraints on the progenitor of SN 2011ht. The grey region is ruled out by the SDSS fluxes. The blue closed circles are known LBVs (mostly Galactic) in their quiescent state, orange triangles are yellow hypergiants, and red open circles are red supergiants (RSGs) in the LMC and SMC. The lines are evolutionary tracks for single stars ($Z=0.004$).

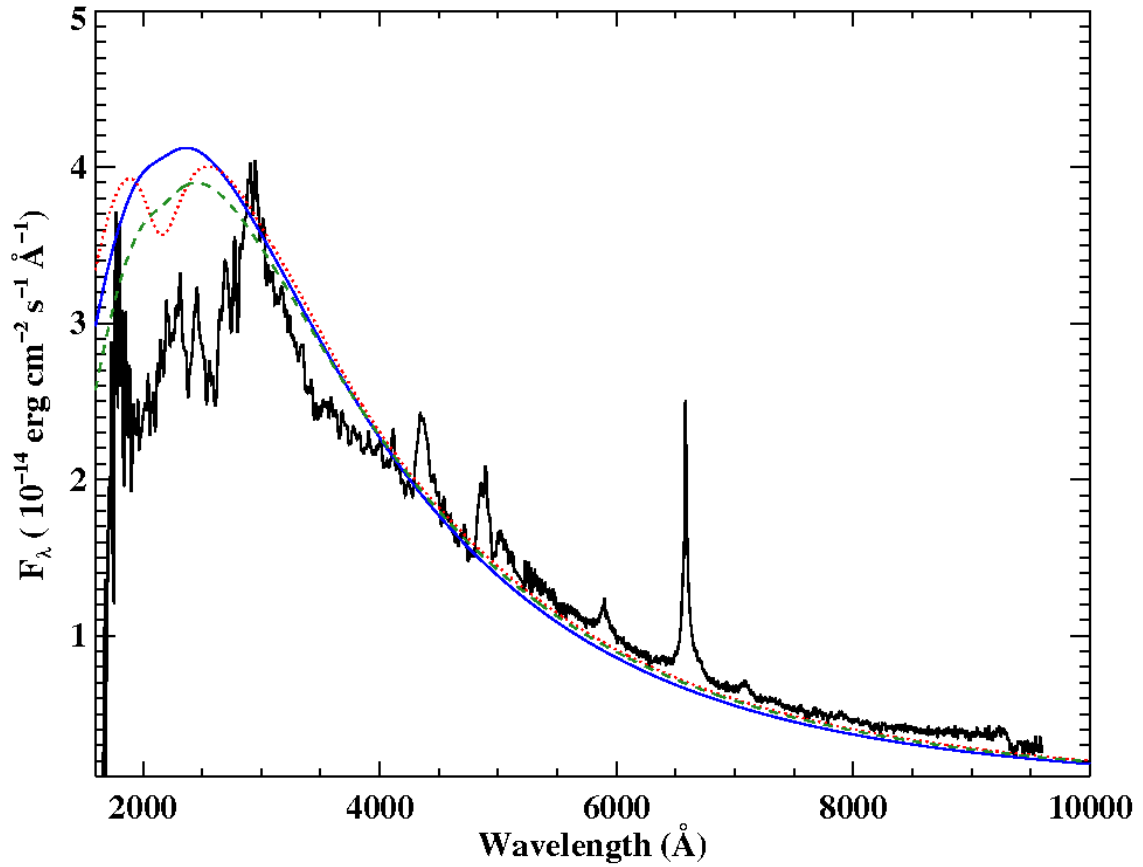


Fig. 7.— Blackbodies (12,900 K) over-plotted on the combined ARC/DIS and UVOT/uvg (Epoch 2) spectrum. The blue solid, red dotted, and green dashed lines represent no, MW ($E(B-V)=0.062$), and SMC ($E(B-V)=0.041$) host reddening, respectively.

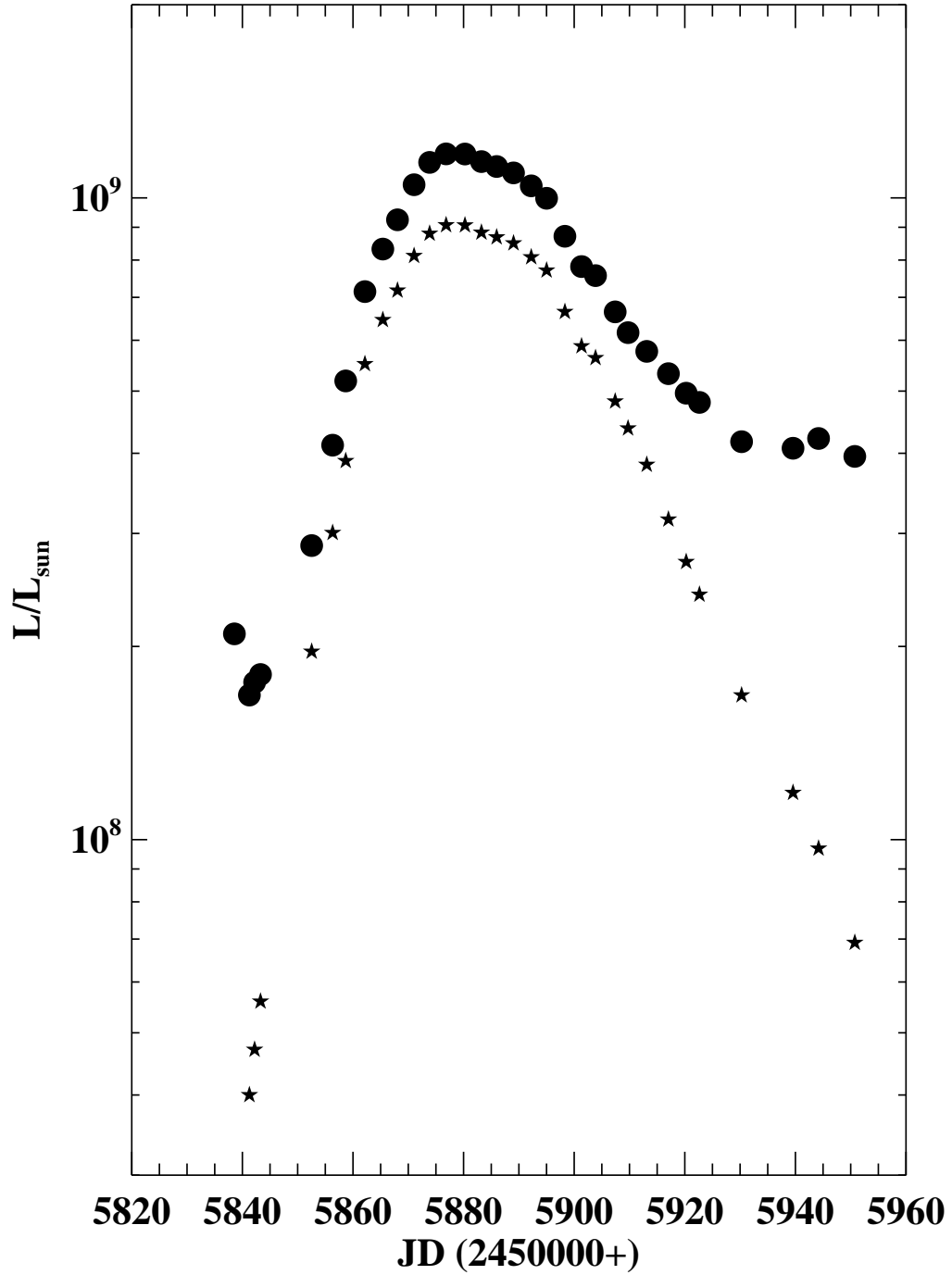


Fig. 8.— Bolometric (circles) and pseudo-bolometric (stars) light curves generated from the UVOT photometric data. SEDs are fitted as blackbodies to determine the bolometric luminosity. Pseudo-bolometric luminosities are calculated by summing the observed fluxes.

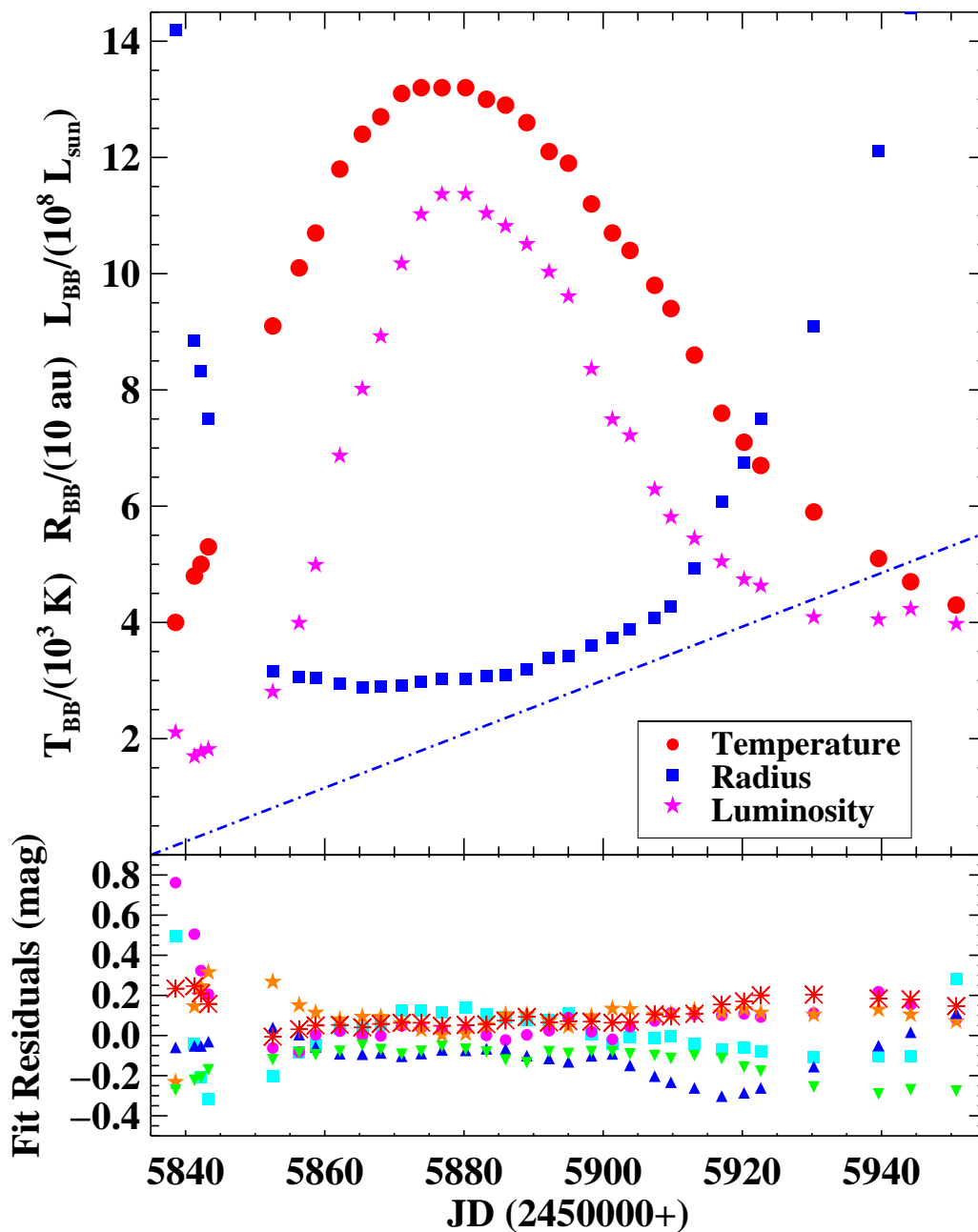


Fig. 9.— Blackbody temperature, radius, and luminosity with the corresponding residuals to the blackbody fits. The diagonal line in the upper panel represents 800 km s^{-1} expansion.

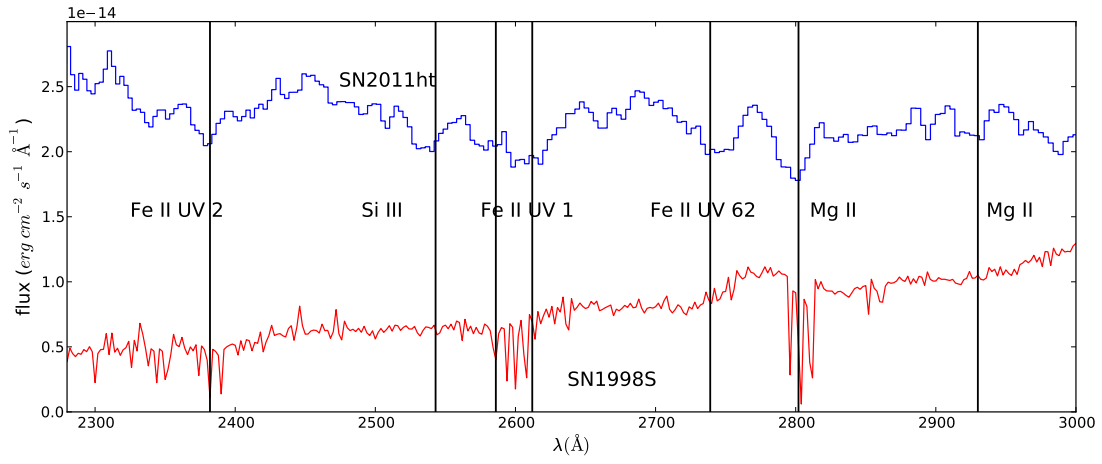


Fig. 10.— *Swift* UVOT/uvg spectrum of SN 2011ht as compared to the spectrum of SN 1998S (Bowen et al. 2000). The red spectrum is of SN 1998S and the blue is of SN 2011ht (UVOT/uvg Epoch 2).

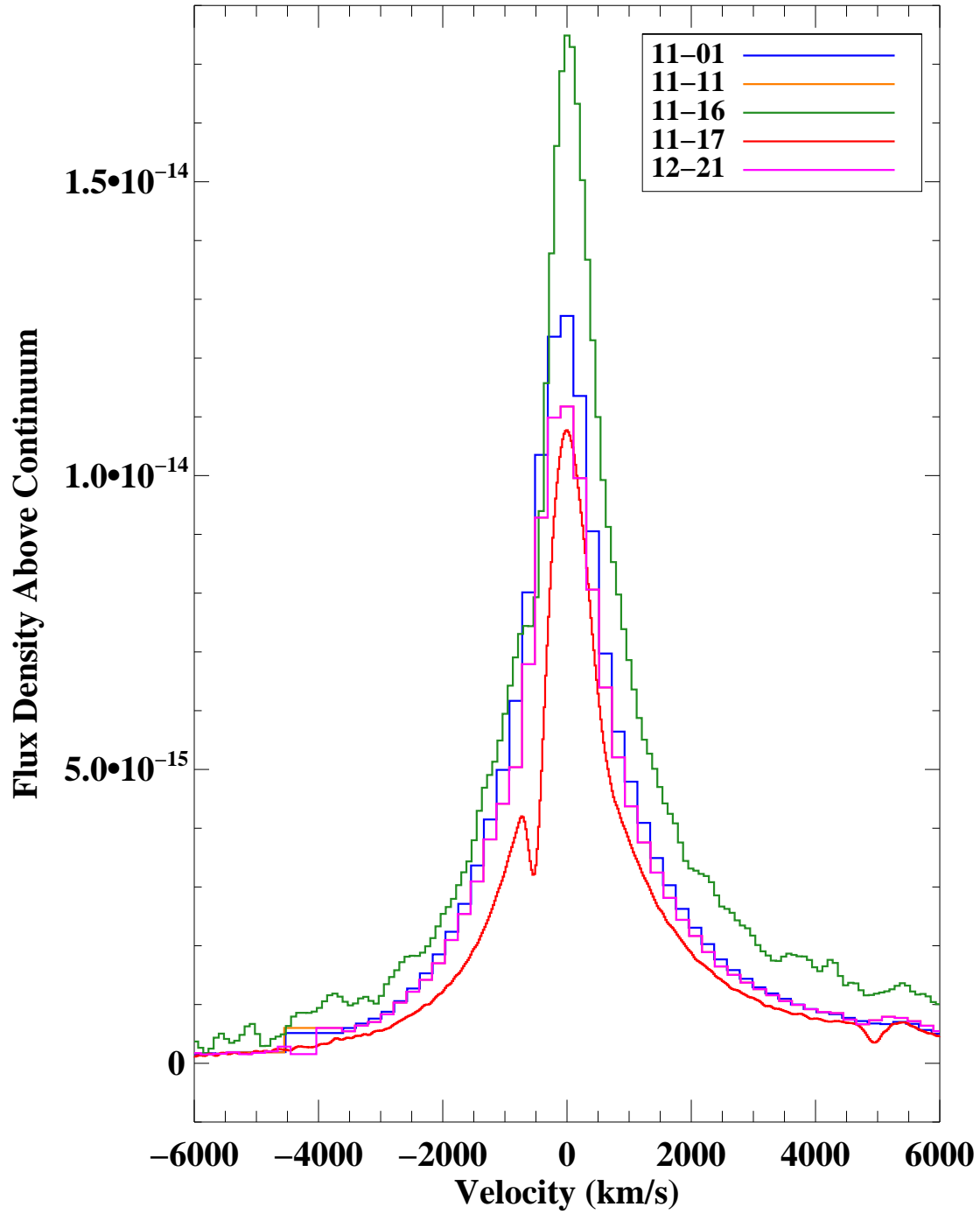


Fig. 11.— $H\alpha$ profile at each spectral epoch plotted in velocity space. The emission peaks have been aligned to zero velocity. The coarseness of the plots represents the resolution of the individual instruments.

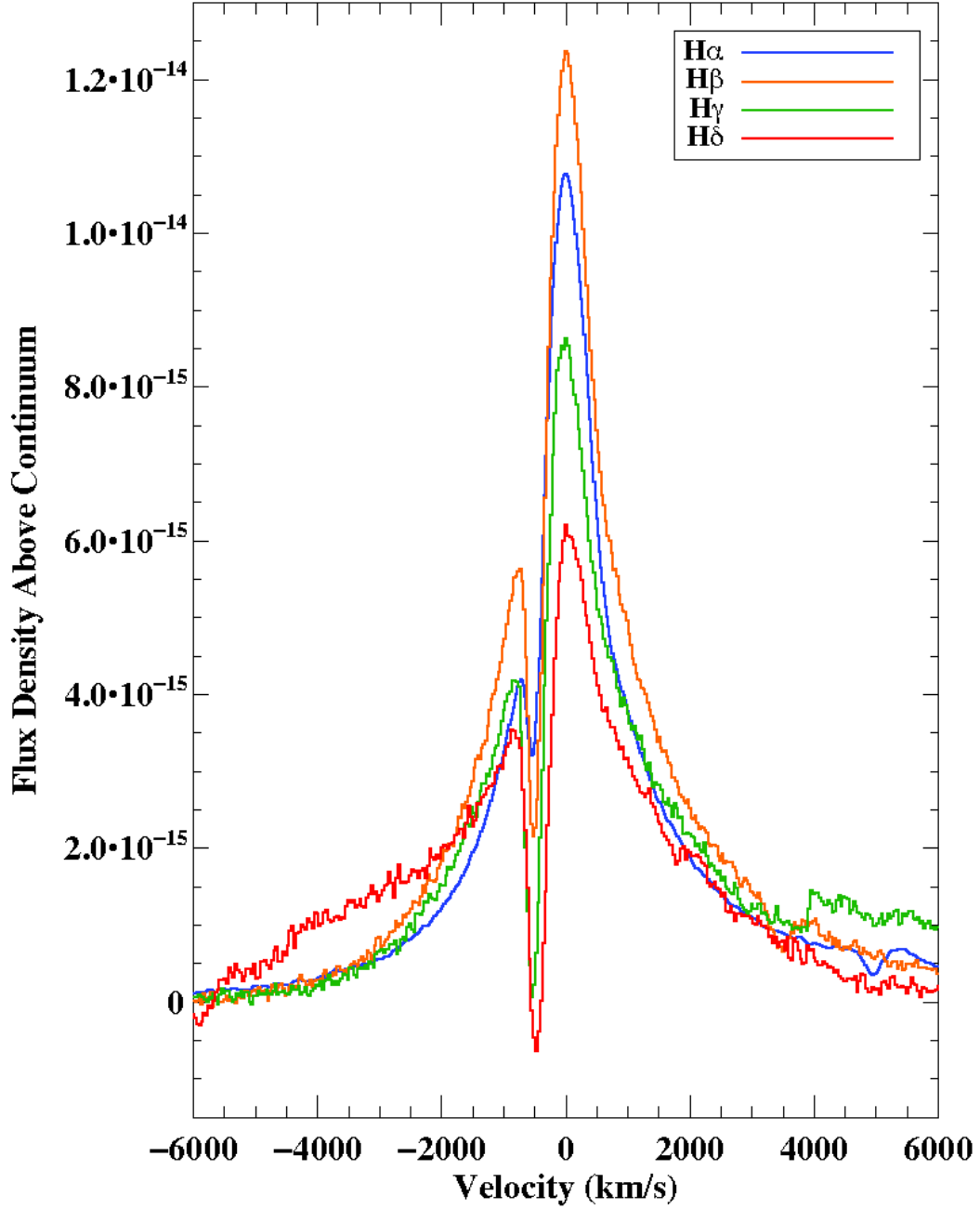


Fig. 12.— Balmer profiles for the LBT/MODS1 spectrum overlaid in velocity space. The emission peaks have been aligned to zero velocity.

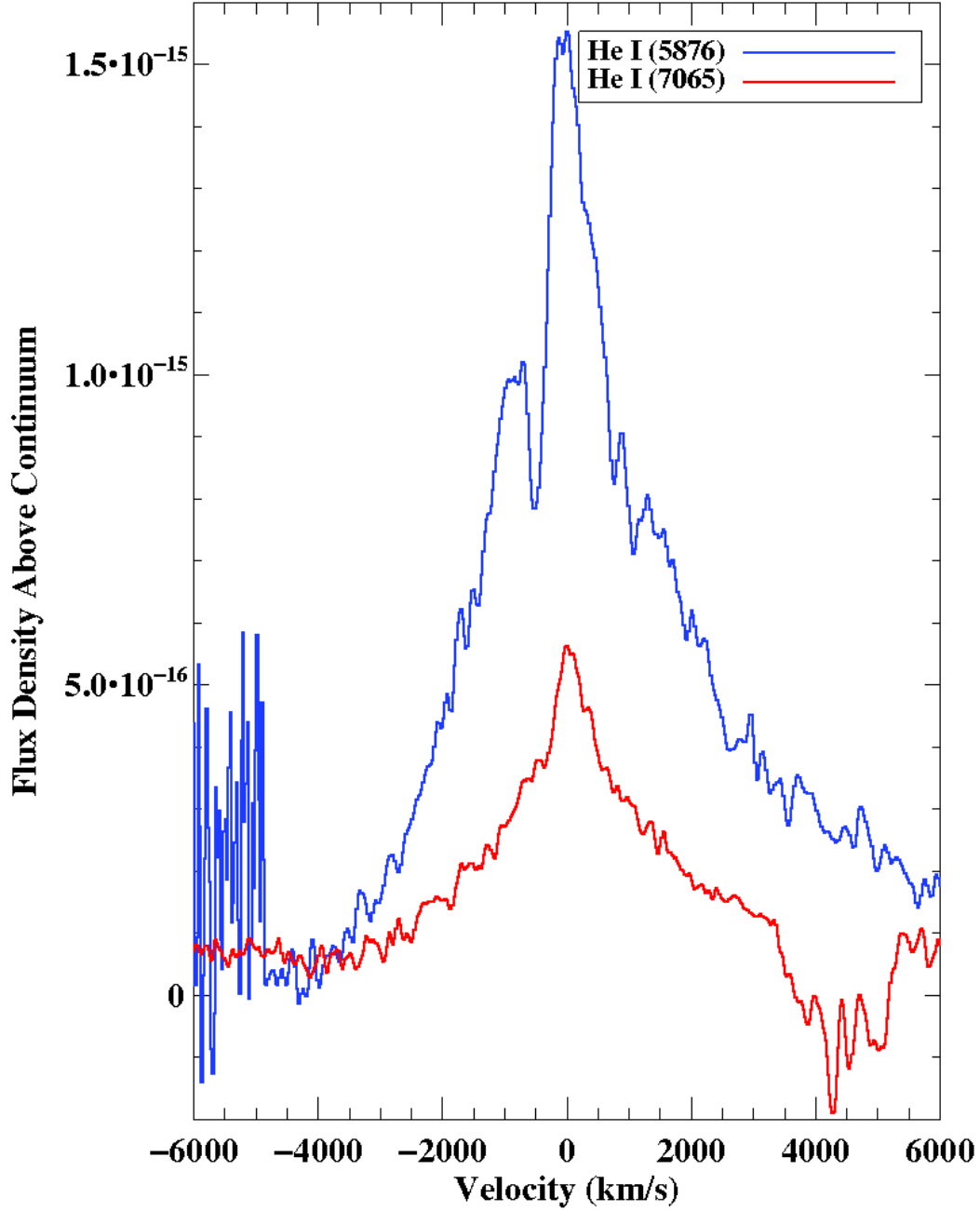


Fig. 13.— The He I emission lines ($\lambda 7065$ and $\lambda 5876$) plotted in velocity space. Note the broad wings in both lines and the absorption similar to hydrogen in the $\lambda 5876$ profile but missing in $\lambda 7065$.

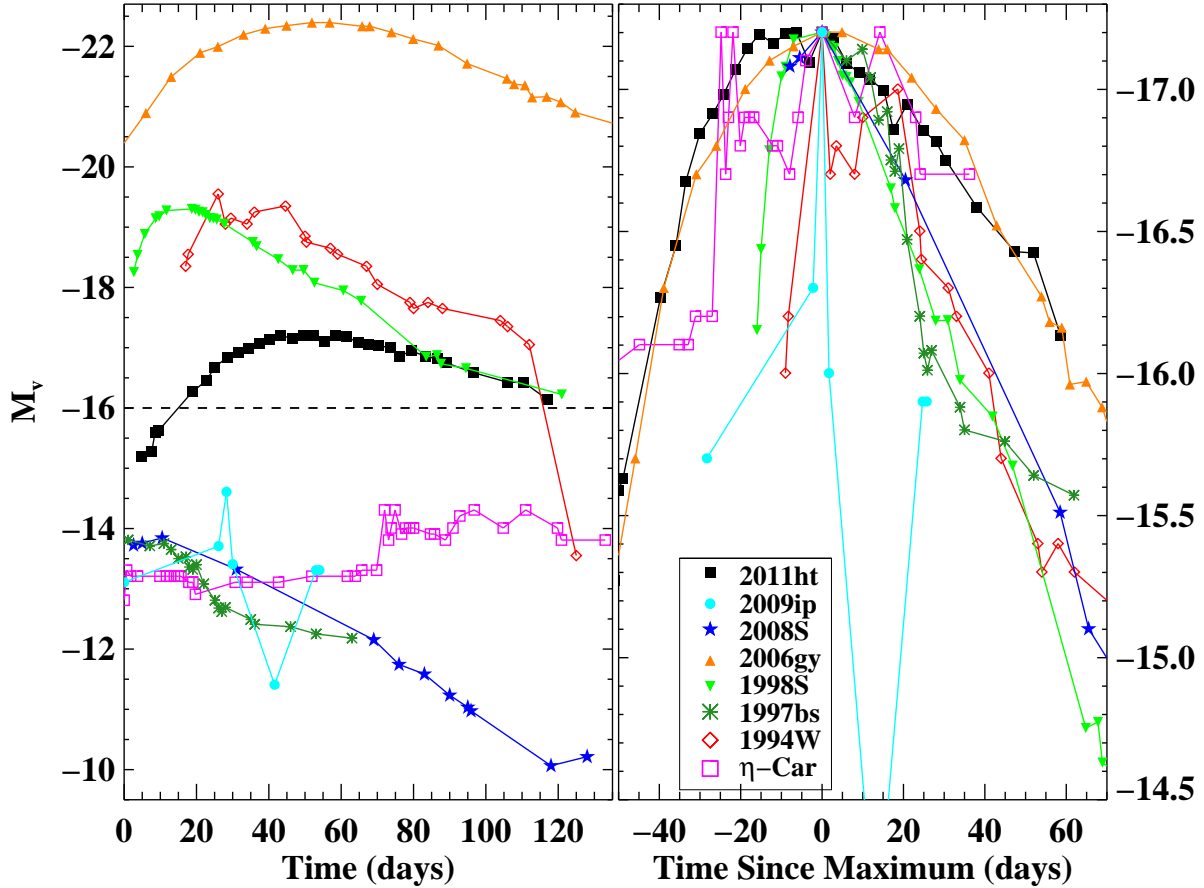


Fig. 14.— Comparison of the SN 2011ht light curve to the SNe IIn light curves of SNe 2006gy (Smith et al. 2007), 1998S (Liu et al. 2000), and 1994W (Sollerman et al. 1998) and the SN impostor light curves of SN 2009ip (Smith et al. 2010b), SN 2008S (Smith et al. 2009), SN 1997bs (Van Dyk et al. 2000) and the 1843 outburst of η Car (Smith & Frew 2011). *Left:* A comparison of the absolute magnitude assuming distance moduli for SNe 2011ht, 2006gy, 1998S, 1994W, 2009ip, 2008S, 1997bs, and η -Car of 31.42, 34.42, 31.15, 32.02, 31.55, 28.74, 30.28, and 11.81, and an $E(B - V)$ of 0.062, 0.76, 0.15 (Lentz et al. 2001), 0.17, 0.019, 0.64, 0.21, and $A_V = 1.7$ (Davidson & Humphreys 1997), respectively. For all objects except η -Car the times have been shifted in order that the day of discovery equals zero. For η -Car, the shift was chosen to coincide with the outburst of 1843. The dotted line is the upper most limit for the peak magnitude of the GE-LBV sample by Smith et al. (2011b). *Right:* A comparison of light curve shapes. All light curves have been shifted so their peak magnitudes coincide with the peak of SN 2011ht. The temporal (and magnitude) shifts for SNe 2011ht, 2006gy, 1998S, 1994W, 2009ip, 2008S, 1997bs, and η -Car are 52.3 (0), 51.9 (+5.17), 18.7 (+2.08), 26.0 (+2.33), 28.3 (-2.61), 10.5 (-3.38), 1.1 (-3.41), and 72.0 (-2.91). The peak for η -Car was chosen to be the middle peak of the four major spikes. The light curves for SNe 2006gy and 2009ip are based primarily on R , not V , band data.

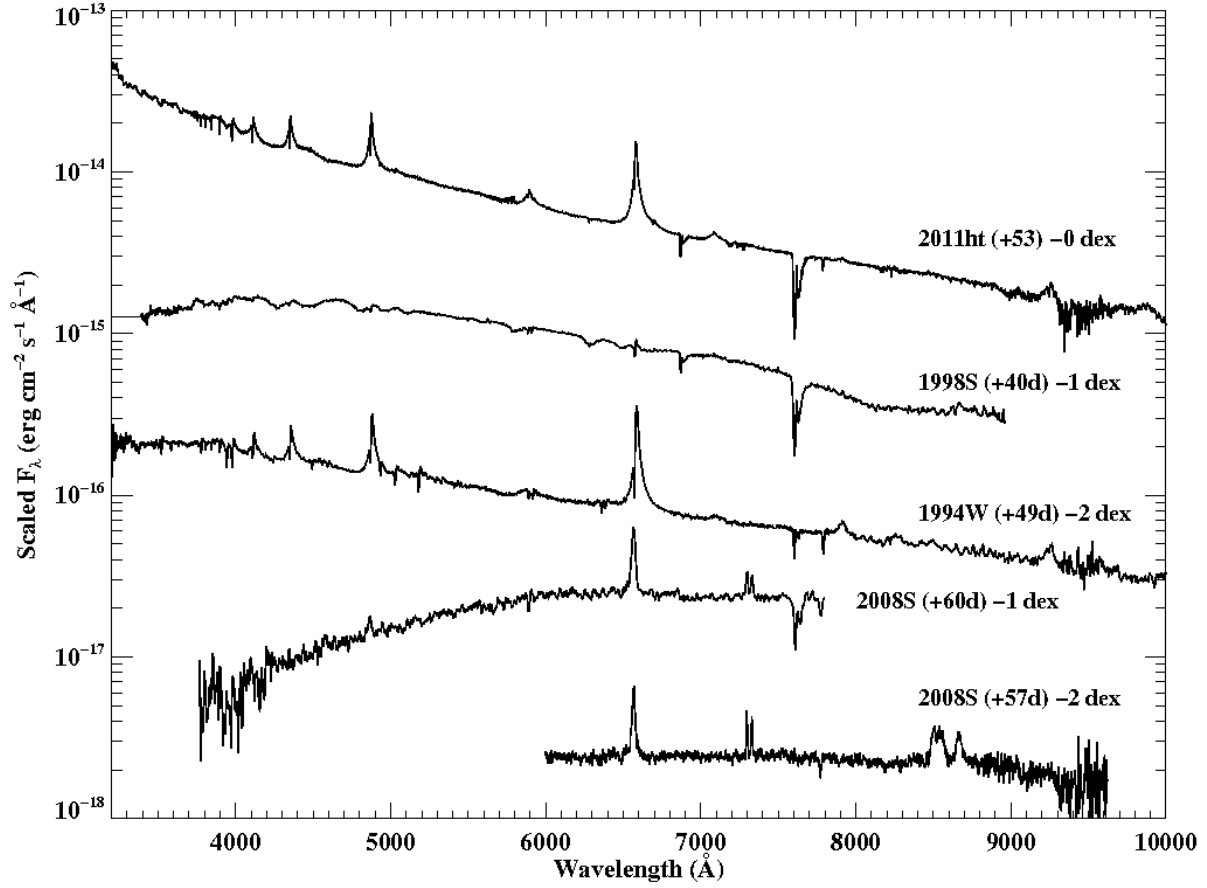


Fig. 15.— Comparison of the SN 2011ht spectrum to the SNe IIn spectra of SNe 1998S and 1994W (Chugai et al. 2004) and the SN impostor’s spectra of SN 2008S (Botticella et al. 2009). The SN 2008S +60 d spectrum was redshifted by 269\AA to match the $H\alpha$ peak of the +57 d spectrum.

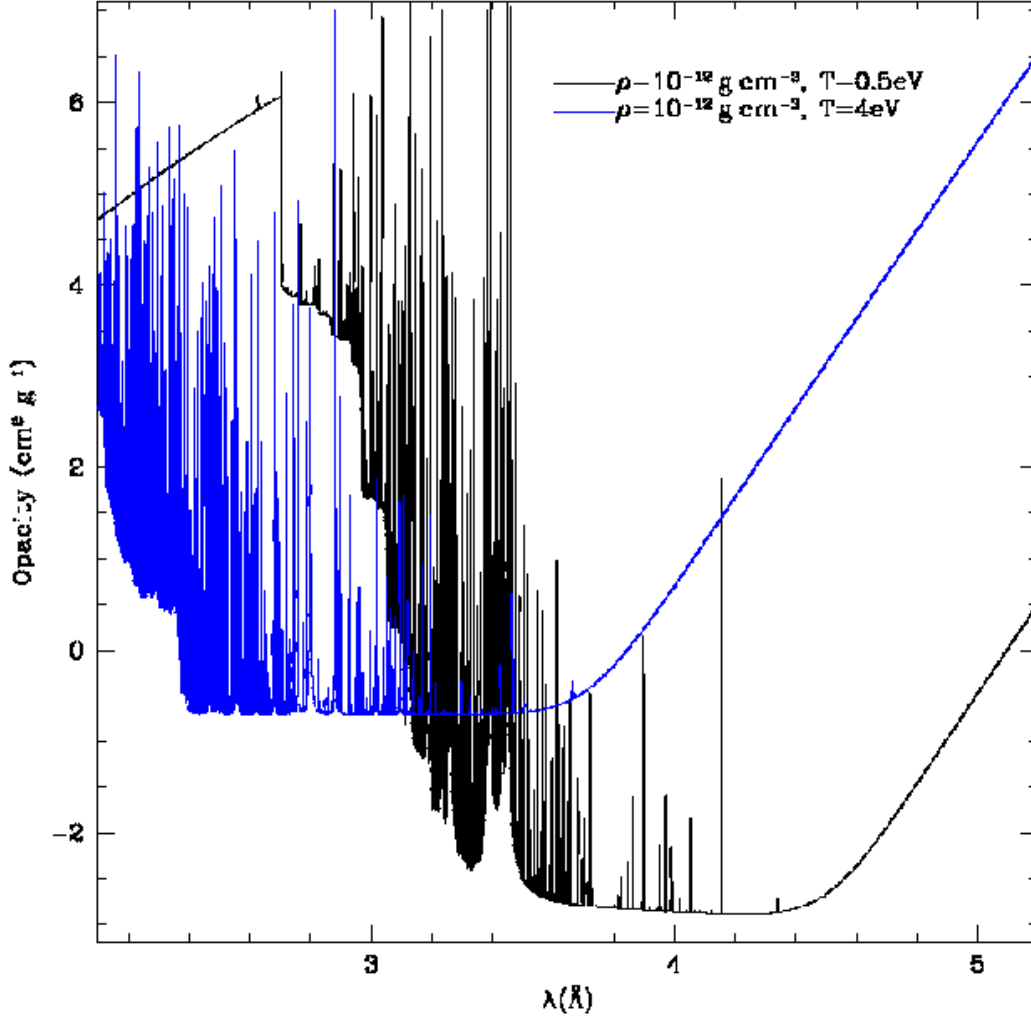


Fig. 16.— Wavelength dependent opacity for a density of $10^{-12} \text{ g cm}^{-3}$ at two different temperatures: 4 eV (blue), 0.5 eV (black). As the shell drops below a temperature of 1 eV, recombination drastically increases the opacity below a few thousand \AA while decreasing the electron scattering opacity (as the number of free electrons diminishes). In this way, the X-ray optical depth can be very high while maintaining a modest optical depth in the optical bands. The opacities are from the LANL OPLIB database (Magee et al. 1995).

Table 1. *Swift* UVOT and ASAS-SN photometry of SN 2011ht

UT (JD2450000+)	Instrument	Observed Magnitudes ^a					
		<i>uvw2</i>	<i>uvm2</i>	<i>uvw1</i>	<i>u</i>	<i>b</i>	<i>v/V</i> ^b
5838.6	UVOT	21.01(46)	20.24(**)	19.07(16)	17.74(09)	17.14(07)	16.45(07)
5841.3	UVOT	20.37(42)	20.39(**)	18.42(14)	16.95(09)	16.72(07)	16.37(09)
5842.2	UVOT	19.37(21)	19.80(27)	18.32(14)	16.69(09)	16.62(07)	16.05(08)
5843.3	UVOT	18.68(14)	19.13(18)	18.01(12)	16.45(08)	15.41(07)	16.01(08)
5852.5	UVOT	15.70(15)	15.50(09)	15.40(10)	14.84(11)	15.50(10)	15.37(09)
5856.3	UVOT	15.13(17)	14.94(15)	14.78(12)	14.43(11)	15.25(09)	15.19(07)
5857.07	ASAS-SN	–	–	–	–	–	15.00(02)
5857.08	ASAS-SN	–	–	–	–	–	15.04(02)
5857.09	ASAS-SN	–	–	–	–	–	15.01(02)
5857.10	ASAS-SN	–	–	–	–	–	15.03(02)
5858.08	ASAS-SN	–	–	–	–	–	14.97(02)
5858.09	ASAS-SN	–	–	–	–	–	14.96(02)
5858.10	ASAS-SN	–	–	–	–	–	14.93(02)
5858.11	ASAS-SN	–	–	–	–	–	14.94(02)
5858.12	ASAS-SN	–	–	–	–	–	14.94(02)
5858.13	ASAS-SN	–	–	–	–	–	14.93(02)
5858.14	ASAS-SN	–	–	–	–	–	14.96(02)
5858.7	UVOT	14.67(20)	14.46(11)	14.35(14)	14.09(12)	15.02(10)	14.97(07)
5859.06	ASAS-SN	–	–	–	–	–	14.96(02)
5859.07	ASAS-SN	–	–	–	–	–	14.96(02)
5859.09	ASAS-SN	–	–	–	–	–	14.92(02)
5859.10	ASAS-SN	–	–	–	–	–	14.94(02)
5859.11	ASAS-SN	–	–	–	–	–	14.98(02)
5862.06	ASAS-SN	–	–	–	–	–	14.76(01)
5862.07	ASAS-SN	–	–	–	–	–	14.74(01)
5862.08	ASAS-SN	–	–	–	–	–	14.74(01)
5862.10	ASAS-SN	–	–	–	–	–	14.76(01)
5862.11	ASAS-SN	–	–	–	–	–	14.74(01)
5862.13	ASAS-SN	–	–	–	–	–	14.70(01)
5862.14	ASAS-SN	–	–	–	–	–	14.73(01)
5862.15	ASAS-SN	–	–	–	–	–	14.73(01)
5862.2	UVOT	14.26(23)	14.05(19)	13.97(16)	13.74(12)	14.77(10)	14.80(08)
5864.06	ASAS-SN	–	–	–	–	–	14.69(01)
5864.07	ASAS-SN	–	–	–	–	–	14.67(01)
5864.08	ASAS-SN	–	–	–	–	–	14.70(01)
5864.11	ASAS-SN	–	–	–	–	–	14.64(01)
5864.12	ASAS-SN	–	–	–	–	–	14.64(01)
5864.13	ASAS-SN	–	–	–	–	–	14.66(01)
5864.14	ASAS-SN	–	–	–	–	–	14.64(01)
5864.15	ASAS-SN	–	–	–	–	–	14.64(02)
5865.4	UVOT	13.96(27)	13.73(21)	13.62(19)	13.55(13)	14.66(11)	14.73(08)
5868.1	UVOT	13.89(21)	13.62(19)	13.67(14)	13.52(10)	14.64(09)	14.66(07)
5871.1	UVOT	13.67(30)	13.45(28)	13.38(20)	13.36(14)	14.44(11)	14.57(08)
5873.9	UVOT	13.68(24)	13.41(23)	13.29(17)	13.27(12)	14.41(10)	14.50(08)
5876.8	UVOT	13.55(27)	13.31(25)	13.21(19)	13.27(12)	14.37(10)	14.45(08)

Table 1—Continued

UT (JD2450000+)	Instrument	Observed Magnitudes ^a					
		<i>uvw2</i>	<i>uvm2</i>	<i>uvw1</i>	<i>u</i>	<i>b</i>	<i>v/V</i> ^b
5880.3	UVOT	13.62(30)	13.37(28)	13.23(21)	13.28(13)	14.39(11)	14.48(08)
5883.2	UVOT	13.64(30)	13.35(26)	13.28(21)	13.29(13)	14.36(11)	14.45(08)
5886.0	UVOT	13.66(29)	13.38(27)	13.40(19)	13.32(12)	14.37(11)	14.44(08)
5889.0	UVOT	13.71(22)	13.47(20)	13.44(15)	13.31(11)	14.32(09)	14.55(07)
5892.2	UVOT	13.81(28)	13.55(26)	13.47(19)	13.30(13)	14.39(11)	14.44(08)
5895.0	UVOT	13.96(27)	13.71(23)	13.55(19)	13.36(13)	14.44(11)	14.46(08)
5898.3	UVOT	14.09(19)	13.87(17)	13.66(14)	13.43(10)	14.45(09)	14.55(07)
5901.4	UVOT	14.76(12)	14.27(11)	14.06(12)	13.67(10)	14.63(08)	14.59(07)
5903.9	UVOT	14.48(23)	14.24(21)	14.02(17)	13.62(14)	14.60(11)	14.61(08)
5907.4	UVOT	14.70(16)	14.53(13)	14.22(12)	13.64(10)	14.66(09)	14.65(07)
5909.8	UVOT	15.02(18)	14.81(16)	14.45(14)	13.84(12)	14.80(10)	14.78(08)
5913.1	UVOT	15.32(13)	15.14(11)	14.68(10)	13.88(10)	14.78(09)	14.70(07)
5917.0	UVOT	15.83(11)	15.64(09)	15.09(09)	14.08(09)	14.92(08)	14.79(07)
5920.2	UVOT	16.38(10)	16.20(08)	15.45(08)	14.30(09)	14.96(08)	14.83(07)
5922.6	UVOT	16.53(10)	16.37(08)	15.63(08)	14.45(09)	15.03(08)	14.89(07)
5930.3	UVOT	17.43(10)	17.44(08)	16.32(08)	15.05(08)	15.25(08)	15.06(07)
5939.6	UVOT	18.36(12)	18.54(12)	17.15(09)	15.77(08)	15.58(07)	15.21(07)
5944.2	UVOT	18.77(15)	19.26(19)	17.53(10)	16.07(08)	15.73(07)	15.22(07)
5950.7	UVOT	19.96(29)	19.95(**)	18.18(12)	16.79(08)	16.15(07)	15.50(07)

^aThe first two *uvm2* values are 2σ -level detections. Values in parenthesis are the errors. 3σ upper limits are marked with **.

^bThe *v/V* column indicates the UVOT/ASAS-SN filter.

Table 2. Spectroscopic Observations of SN 2011ht

Instrument	Date (UT)	Exposure (s)
HET/LRS	2011-11-01	600.00
UVOT/uv _g	2011-11-02	3710.08
ARC/DIS	2011-11-11	1200.00
UVOT/uv _g	2011-11-13	15,550.70
HET/LRS	2011-11-16	600.00
LBT/MODS1	2011-11-17	900.00
HET/LRS	2011-12-21	600.00

Table 3. SN 2011ht host galaxy properties

Parameter	Value	Note/Reference
Name	UGC 5460	NED
R. A. (J2000)	$10^h 08^m 09^s.3$	NED
Dec. (J2000)	$+51^\circ 50' 38'' 0$	NED
Morphological Type	SB(rc)d	de Vaucouleurs et al. (1991); Corwin et al. (1994)
Heliocentric velocity	1093 km s^{-1}	NED
Virgo-infall corrected velocity	1403 km s^{-1}	NED
Distance modulus	31.42 mag	using $d_{\text{flow}} = 19.2 \text{ Mpc}$
M_B	-18.0 mag	this paper
Total SFR	$1.2^{+3.5}_{-1.0} \text{ M}_\odot \text{ yr}^{-1}$	this paper
Total M_\star	$1.1^{+0.5}_{-0.4} \times 10^9 \text{ M}_\odot$	this paper
Total A_V	$0.8^{+0.6}_{-0.8} \text{ mag}$	this paper
Oxygen abundance	8.20	Pettini & Pagel (2004) $O3N2$ method, this paper

Table 4. SN 2011ht Blackbody and Bolometric Data

UT (JD2450000+)	T_{BB} (K)	R_{BB} ($\times 10^{14}$ cm)	L_{BB} ($\times 10^{42}$ erg s $^{-1}$)	L_{Pseudo} ($\times 10^{42}$ erg s $^{-1}$)	$L_{\text{Bolometric}}$ ($\times 10^{42}$ erg s $^{-1}$)	χ^2_{ν}
5838.56	4000	21.23	0.82	0.11	0.81	43.62
5841.27	4800	13.23	0.66	0.16	0.66	22.96
5842.21	5000	12.46	0.69	0.18	0.69	21.40
5843.28	5300	11.24	0.71	0.22	0.71	22.76
5852.53	9100	4.74	1.10	0.77	1.12	11.47
5856.32	10100	4.59	1.56	1.18	1.61	3.03
5858.69	10700	4.57	1.95	1.52	2.03	2.30
5862.16	11800	4.40	2.68	2.15	2.79	2.05
5865.40	12400	4.31	3.13	2.52	3.25	1.30
5868.05	12700	4.33	3.48	2.80	3.61	2.61
5871.05	13100	4.34	3.96	3.17	4.09	2.12
5873.86	13200	4.46	4.29	3.43	4.43	2.30
5876.84	13300	4.48	4.47	3.54	4.58	1.22
5880.25	13200	4.53	4.43	3.54	4.57	1.23
5883.23	13000	4.60	4.31	3.44	4.44	1.35
5885.98	12900	4.62	4.22	3.38	4.35	2.85
5889.03	12600	4.78	4.10	3.31	4.26	5.40
5892.23	12100	5.06	3.91	3.15	4.07	2.08
5895.01	11900	5.13	3.75	3.01	3.90	2.74
5898.32	11200	5.40	3.26	2.60	3.40	3.42
5901.33	10700	5.60	2.92	2.29	3.05	4.23
5903.86	10400	5.82	2.82	2.20	2.95	3.36
5907.41	9800	6.11	2.45	1.88	2.59	8.91
5909.74	9400	6.38	2.27	1.71	2.41	7.24
5913.12	8600	7.38	2.13	1.50	2.25	12.88
5917.04	7600	9.11	1.97	1.23	2.08	20.37
5920.25	7100	10.11	1.85	1.06	1.94	25.87
5922.65	6700	11.22	1.81	0.94	1.87	27.09
5930.27	5900	13.59	1.59	0.65	1.62	27.72
5939.57	5100	18.09	1.58	0.46	1.58	29.41
5944.19	4700	21.77	1.65	0.38	1.64	23.15
5950.74	4300	25.23	1.55	0.27	1.54	22.78

Table 5. Blueshifted^a Line Measurements for SN 2011ht^b

Spectral Line	Emission (km s ⁻¹)	Absorption (km s ⁻¹)
H α	261	778
H β	211	747
H γ	194	706
H δ	157	676
H ϵ	96	670
H ζ	129	646
H η	—	646
He I		
7065	218	—
6678	145	558
5876	148	603
5015	106	519
4922	81	502
4471	217	563
4026	—	609
3819	—	606
O I		
7774	—	618
Ca II K	—	643

^aRelative to the heliocentric velocity of the galaxy.

^bThese values correspond to the MODS1 spectrum in Figure 3.